Macrophages stimulate epicardial VEGFaa expression to trigger cardiomyocyte proliferation in larval zebrafish heart regeneration

Finnius A. Bruton[1]*, Aryan Kaveh[1], Katherine M. Ross-Stewart[1], Gianfranco Matrone[1], Magdalena E.M. Oremek[2], Emmanouil G. Solomonidis[1], Carl S. Tucker[1], John J. Mullins[1], Mairi Brittan[1], Jonathan M. Taylor[3], Adriano G. Rossi[2], Martin A. Denvir[1].

[1]Centre for Cardiovascular Science, Queen's Medical Research Institute, University of Edinburgh, Edinburgh, United Kingdom.

[2]Centre for Inflammation Research, Queen's Medical Research Institute, University of Edinburgh, Edinburgh, United Kingdom.

[3]Department of Physics, University of Glasgow, Glasgow, United Kingdom.

Corresponding author: *

Abstract

Cardiac injury induces a sustained macrophage response in both zebrafish and mammals. Macrophages perform a range of both beneficial and detrimental functions during mammalian cardiac repair, yet their precise roles in zebrafish cardiac regeneration are not fully understood. Here we characterise cardiac regeneration in the rapidly regenerating larval zebrafish laser injury model and use macrophage ablation and macrophage-null *irf8* mutants to define the role of macrophages in key stages of regeneration. Live heartbeat-synchronised imaging and RNA sequencing revealed an early proinflammatory phase, marked by tnfa+ macrophages, which then resolved to an anti-inflammatory, profibrotic phase. Macrophages were required for cardiomyocyte proliferation but not for functional or structural recovery following injury. Importantly, we found that macrophages are specifically recruited to the epicardial-myocardial niche, triggering the expansion of the epicardium which upregulates VEGFaa expression to induce cardiomyocyte proliferation. Hence, revealing a novel mechanism by which macrophages facilitate cardiac regeneration.

Introduction

Zebrafish are highly regenerative, exhibiting the capacity to restore full structure and function to a wide range of tissues following injury[1–5]. Cardiac injury is one such example where adult mammals are only able to facilitate maladaptive repair but zebrafish exhibit full tissue regeneration[6,7]. In humans, the most severe form of cardiac injury is myocardial infarction (MI), where occlusion of a coronary artery triggers ischemic injury to the myocardium, leading to the loss of approximately 1 billion cardiomyocytes[8]. Adult mammalian cardiomyocytes are considered largely post-mitotic, switching to hypertrophic growth shortly after birth. They are therefore unable to restore lost myocardium, which is instead replaced with non-contractile scar tissue[9]. Consequently, MI patients suffer sequalae of maladaptive remodelling, leading to left ventricular dilation and thinning of the scar, further decreasing the function of the heart[10,11]. Hence, there is a need for medical innovation which can reverse or prevent this process.

In contrast to mammalian models of MI, apical resection and cryoinjury MI models in zebrafish show full regeneration of lost myocardium *via* the dedifferentiation and proliferation of surviving cardiomyocytes[12,13]. Cardiac regeneration is complex and dynamic, with zebrafish hearts undergoing debridement of dead myocardium, followed by transient fibrosis, revascularisation and eventual replacement of cardiomyocytes[14]. The inflammatory response has been demonstrated to be crucial for each of these key events, both in zebrafish and also in other regenerative species such as axolotls and neonatal mice[15–17]. In particular, macrophages have emerged as important cellular regulators of tissue regeneration. Indeed, macrophage ablation has been shown to abrogate regeneration across multiple organs and organisms, including the adult zebrafish heart[15,16,18]. However, the precise contribution of macrophages to cardiac repair has been complicated by disparate results following macrophage perturbation in mouse models of MI, where macrophages have been reported to be both beneficial and detrimental[7,19,20]. This is in part attributed to substantial heterogeneity of macrophage subtypes, and phenotypic plasticity[21,22]. Recent studies have confirmed the presence of macrophage subsets in zebrafish, yet their functional niche and interactions with other key cell types of the heart, such as the epicardium, remain poorly understood[23,24]. The larval zebrafish model of cardiac regeneration offers a tractable system to examine macrophages in detail. Larval zebrafish regenerate more

rapidly than adults, occurring in just 48 hours after cardiac laser injury in 3-day old larvae[25,26]. Combined with their amenability for live *in vivo* imaging and genetic tractability, this model becomes a powerful tool with which to carefully examine how macrophages support multiple aspects of cardiac regeneration.

Here we report an in-depth characterisation of the macrophage response and several key regenerative processes in larval zebrafish cardiac regeneration, finding the heart regeneration program between the larvae and adults to be highly conserved. Abolition of the macrophage response using metronidazole-nitroreductase ablation of macrophages or the macrophage null *irf8*$^{-/-}$ mutant[27], demonstrated a requirement for these cells in removal of apoptotic cells, epicardial activation and cardiomyocyte proliferation. Interestingly, we found that one of the ways macrophages exert their pro-proliferative effect is via epicardial VEGFaa and downstream endocardial notch signalling. Our study reveals that macrophages invade the epicardial-myocardial niche, inducing expansion of epicardial cell numbers which increases epicardial VEGFaa expression, leading to an upregulation of endocardial notch signalling and the cardiac developmental growth pathway.

Results

Macrophages display cellular heterogeneity following cardiac injury

We first assessed macrophage heterogeneity and recruitment dynamics following larval cardiac injury. We crossed the zebrafish pan-macrophage reporter line *Tg(mpeg1:GFP)* with *Tg(csf1ra:gal4;UAS:mCherry-NfsB)* (shortened here to csf1ra: mCherry) (Supplementary Figure 1a). Csf1ra (colony stimulated factor 1 receptor) is a cytokine required for macrophage development and used as a macrophage reporter promoter in mammals[28].

Larval hearts were lasered at the ventricular apex at 72 hours post-fertilisation (hpf) and imaged at 2, 6, 24, and 48 hours post injury (hpi) (Figure 1a). Macrophages migrate to the injured ventricular apex within 2 hours, peak at 6 and maintain elevated numbers until 48 hpi (Figures 1b & 1c). We found that not all recruited macrophages were co-positive for both transgenes, leading to three subsets 1) mpeg1+csf1ra-

100 (19.3±5.1%), 2) mpeg1-csf1ra+ (2.8±2.1%) and 3) mpeg1+csf1ra+ (77.9±5.7%).
101 Similar dynamics were seen for subsets 1 & 3 but since mpeg1-csf1ra+ were
102 exceedingly rare it is not possible to know if the dynamics are likewise similar. Both
103 subsets exhibit a range of morphologies with no overt difference between groups
104 (Figure 1d, Video 1). Importantly, our data demonstrate that larval macrophages
105 recruited to cardiac injury are heterogenous in their marker expression, similar to adult
106 zebrafish[29], and suggest a comparatively complex macrophage response in the larval
107 model.
108
109 **Macrophages display cellular plasticity following cardiac injury**
110
111 To examine if macrophages display plasticity and convert to an inflammatory
112 phenotype in the larval cardiac injury model, we performed cardiac laser injury on
113 *Tg(tnfa:GFP;mpeg1:mCherry)* larvae. (Figure 1e & 1f). Quantification of tnfa+
114 macrophage number revealed a transient tnfa+ subset (19.3±4.9% of mpeg1+
115 macrophages, n=24), found only at the 24 hpi timepoint and rarely in uninjured larvae
116 (Figure 1f & Supplementary figure 1b). We also observed that from 24 hpi,
117 macrophages retract their pseudopods and become spherical, further suggesting a
118 shift in phenotype (Supplementary figure 1e).
119
120 We reasoned that if tnfa+ macrophages were indeed inflammatory macrophages then
121 application of M1-polarisation cytokine IFN-γ would increase their abundance. A single
122 intravenous injection of zebrafish recombinant protein IFN-γ-rel, immediately prior to
123 cardiac injury, increased the proportion of tnfα+mpeg1+ macrophages from
124 26.4±11.0% in PBS injected controls to 78.8±9.5%, supporting the suggestion that
125 these were inflammatory macrophages (Figure 1g & Supplementary figure 1c & 1d).
126
127 Furthermore, *in vivo* imaging live in the beating heart showed recruited macrophages
128 becoming tnfa:GFP+ after arrival at the injured ventricle, confirming that this
129 represents true *in situ* conversion (Figure 1h, Video 2). Taken together, these data
130 show that, as in adults, macrophages display plasticity and become inflammatory in
131 response to cardiac injury, confirming the complexity of the macrophage response in
132 this model.

133

134 **Larval cardiac laser lesions are similar in structure to adult cryoinjury**

135

136 To validate analyses of macrophage function in the larval injury model, we first sought
137 to determine if the laser lesion is comparable to adult cryoinjury and mammalian
138 infarcts. Using the line *Tg(myl7:mKateCAAX;myl7:h2b-GFP)*, which labels
139 cardiomyocyte sarcolemma and chromatin respectively, we observed that, following
140 injury, a circlet of cardiomyocytes with pyknotic nuclei formed (Figure 2a). These
141 pyknotic nuclei were TUNEL+ at 6 hpi, confirming apoptosis and they encircled the
142 GFP- lesion (Figure 2b & 2c). Heartbeat-synchronised LSFM (lightsheet fluorescence
143 microscopy)[30] showed that nuclear condensation occurred extremely rapidly, being
144 identified by 1.5 hpi (Supplementary figure 2a, Video 3).

145

146 We hypothesised that the GFP- epicentre of the laser lesion may contain cells that
147 immediately necrose upon injury. To test this, we labelled necrotic cells by injecting
148 propidium iodide (PI) intravenously immediately following injury (<0.5 hpi). We found
149 that there were indeed PI+ cells in the GFP- region, and PI+ debris scattered across
150 the proximal myocardium from 1 hpi (Figure 2d). Time-lapse imaging of PI-injected,
151 injured *Tg(mpeg1:GFP;myl7:h2b-GFP;myl7:mKateCAAX)* hearts showed that
152 necrotic cells are rapidly cleared within the first 0-2 hpi (Supplementary figure 2b &
153 Video 3). Necrotic cells either disintegrated or were squeezed out from the
154 myocardium into the pericardial cavity, independently of macrophage contact (Video
155 4). Overall, this characterisation confirms the structure of the laser lesion mirrors the
156 necrotic infarct and apoptotic border zone observed in adult zebrafish cryoinjury and
157 mammalian MI[14,31].

158

159 **Macrophages contribute to the removal of apoptotic cardiomyocytes following**
160 **injury**

161

162 We next sought to understand what role macrophages play in the regeneration of the
163 larval heart, which occurs within only 48 hours of the initial injury[25,26]. We used two
164 different methods to induce macrophage-less hearts. Firstly we used the
165 *Tg(csf1ra:gal4;UAS:mCherry-NfsB)* line (abbreviated hereafter to csf1ra:NfsB-
166 mCherry) that expresses a nitroreductase enzyme NfsB in macrophages, which

167 induces cell-specific apoptosis when exposed to prodrug metronidazole[32]
168 (Supplementary figure 3a-d). Macrophage ablation only occurs in larvae expressing
169 the nitroreductase (NTR) *and* in the presence of metronidazole (NTR+met+).
170 Therefore, larvae only expressing the nitroreductase (NTR+met-) or only in the
171 presence of metronidazole (NTR-met+) are used as macrophage-replete control
172 groups. The second method was the use of the macrophage-null *irf8*$^{-/-}$ mutant[27], IRF8
173 being a transcription factor required for macrophage development (Supplementary
174 figure 3e-h).
175
176 To determine if macrophages are required for the removal of apoptotic cells, we
177 performed TUNEL staining on *irf8*$^{-/-}$ and *irf8*$^{+/+}$ *Tg(myl7:h2b-GFP)* larvae at the
178 standard 2, 6, 24, 48 hpi timepoints (Figure 2e & 2g). In injured *irf8*$^{+/+}$ hearts, the
179 number of apoptotic cardiomyocytes significantly increased at 2 hpi and 6 hpi
180 compared to uninjured controls (4.1±0.9 vs 0.0±0.0 and 5.3±1.0 vs 0.1±0.1
181 respectively, n=15-29) but returned to baseline by 24 hpi. However, although injured
182 macrophage-null *irf8*$^{-/-}$ hearts showed a similar initial pattern of cell death at 2 hpi and
183 6 hpi (5.5±0.8 & 5.9±0.9 apoptotic cardiomyocytes respectively), apoptotic
184 cardiomyocyte cells were still present at 24 hpi, only returning to uninjured levels by
185 48 hpi.
186
187 In the macrophage ablation model, we saw a similar pattern of results where the
188 numbers of apoptotic cells were negligible in uninjured hearts of all treatment groups,
189 but peaked at 6 hpi following injury (NTR+met-, NTR-met+ & NTR+met+ =6.4±0.5,
190 6.4±0.5 and 6.0±0.5, n=10-12) (Figure 2f & 2h). By 24 hpi the non-ablated groups no
191 longer possessed significantly increased numbers of TUNEL+ myocardial cells;
192 however, the macrophage-ablated group showed a retention of apoptotic cells at 24
193 hpi (NTR+met+ = 1.5±0.3) that resolved by 48 hpi.
194
195 To verify that macrophages are directly removing myocardial debris, we performed
196 time-lapse imaging of injured *Tg(myl7:GFP;mpeg1:mCherry)* larvae. We observed
197 small GFP+ pieces of myocardial debris near the GFP- lesion being removed and
198 internalised by macrophages (Figure 2i & Supplementary Figure 2c & Video 5),
199 confirming the essential role of macrophages in lesion debridement.

200

201 **Macrophages are not obligatory for structural or functional recovery of the larval**
202 **heart**

203

204 Next, we sought to investigate if macrophages are required for structural and
205 functional recovery of the larval heart following laser-injury. We injured *Tg(myl7:GFP)*
206 larvae following macrophage ablation and acquired serial 3D scans of the cardiac
207 structure of individual larvae by heartbeat-synchronised LSFM (Figure 3a). In all
208 treatment groups, the lesion size was consistent between 2 hpi and 6 hpi, with no
209 difference between groups. By 24 hpi the lesion had almost completely regressed
210 (95% to 37.1μm^2±24.4, n=11-22) in macrophage-replete NTR+met- larvae (Figure 3b).
211 However, for larvae in the macrophage-ablated NTR+met+ and the other
212 macrophage-replete NTR-met+ group, lesion closure was slightly delayed at 24 hpi
213 (73% and 75% to 234.7±59.7 μm^2 and 221.4±84.6 μm^2 respectively). By 48 hpi the
214 lesions of larvae from each group had entirely regressed and luminal surface renders
215 of injured ventricles showed normal trabecular structure (Figure 3a). These results
216 suggest macrophages are not required for lesion closure, but that metronidazole-
217 treatment slightly delays this process.

218

219 Using *Tg(myl7:GFP)* larvae, we acquired lateral-view videos of beating hearts with
220 epifluorescence microscopy and tested if macrophage ablation affected recovery of
221 cardiac function. Immediately following injury at 2 hpi, volumetric ejection fraction was
222 decreased in all groups from 74% in uninjured ventricles to 54% in injured (Figure 3c
223 & Supplementary figure 4a & 4b). Ejection fraction recovered quickly by 6 hpi in all
224 treatment groups, (~78% injured vs ~87% uninjured) and by 24 hpi and 48 hpi injured
225 hearts were functionally indistinguishable from uninjured hearts. These data suggest
226 that injured larval hearts recover their function rapidly, and that this recovery is not
227 macrophage dependent.

228

229 We next performed identical experiments examining the recovery of cardiac structure
230 and function with *Tg(myl7:GFP)* larvae on an *irf8* mutant background. Both *irf8*$^{+/+}$ and
231 *irf8*$^{-/-}$ genotype larvae showed substantial lesion regression (~80%) between 6 hpi and
232 24 hpi (898.6 μm^2±189.7 to 211.6 μm^2±115.8 vs 1002.9 μm^2±158.4 to 113.89

233 μm^2±59.5, respectively) (Figure 3d & 3e). No difference in lesion size was seen at any
234 timepoint and both genotypes had completely closed their lesions by 48 hpi. Normal
235 trabecular structure was seen in both groups at 48 hpi following full structural recovery
236 (Figure 3d). The recovery of ejection fraction in this model followed the same trend as
237 that of the metronidazole-nitroreductase model, with the ejection fraction of injured
238 larvae being indistinguishable from uninjured larvae by 24 hpi in both genotypes
239 (Figure 3f). Our near identical findings in the *irf8* macrophage null model confirm that
240 larval hearts rapidly recover following laser injury and that this process is macrophage
241 independent.
242
243 Finally, we wished to understand the mechanism of lesion closure. We performed
244 heartbeat-synchronised time-lapse imaging of lesions in *Tg(myl7:GFP)* larvae
245 immediately following injury. We observed GFP+ myocardial budding on opposite
246 sides of the lesion border zone and subsequent invasion into the lesion, adhering to
247 each other to form bridges (Figure 3g, Video 6). Repeating this experiment in
248 *Tg(myl7:h2b-GFP;myl7:mKateCAAX)* larvae facilitated the tracking of individual
249 cardiomyocytes by virtue of their labelled nuclei and plasma membranes (Video 7 &
250 Supplementary figure 2d). We found that cardiomyocytes bordering the lesion did not
251 divide but extended protrusions into the lesion until they adhered with other single
252 cardiomyocytes bridging from the opposing side of the lesion. These imaging insights
253 suggest that myocardial structure is first restored by morphogenesis rather than cell
254 division.
255
256 **Macrophage ablation abolishes an injury-associated increase in cardiomyocyte**
257 **proliferation**
258
259 To test if cardiomyocyte proliferation increases in response to laser-injury, we
260 performed EdU staining in *Tg(myl7:h2b-GFP)* larvae in two experiments. In the first
261 experiment, uninjured and injured larvae were exposed to EdU during 0-24 hpi and
262 then at 24-48 hpi for the second (Figure 4a). Comparison between uninjured and
263 injured hearts revealed no significant difference in the proportion of EdU+
264 cardiomyocyte nuclei 0-24 hpi (21.3±3.3 vs 18.9±3.4 respectively, n=10-14) (Figure
265 4b & 4c). However, over 24-48 hpi there was an organ-wide, 35% increase in the

266 proportion of EdU+ cardiomyocytes in injured hearts relative to uninjured (43.5±1.8%
267 vs 32.2±2.0% respectively, n=17-25). Time-lapse *in vivo* imaging of dividing
268 cardiomyocytes showed nuclear division followed by cytokinesis, exclusively gives rise
269 to mononuclear cells, with no obvious hypertrophy (Video 8, Supplementary Figure
270 5a).
271
272 To understand if macrophages are required for the injury-dependent increase in
273 cardiomyocyte proliferation, EdU was pulsed during the proliferative 24-48 hpi window
274 in the macrophage-less models (Figure 4d). In the metronidazole-nitroreductase
275 ablation model we found that the percentage of EdU+ cardiomyocytes increased in
276 injured hearts in both the NTR+met- and NTR-met+ control groups, but not in the
277 macrophage-ablated NTR+met+ group (Figure 4e & 4f). This result indicates that
278 macrophages are a requirement for injury-dependent increase in cardiomyocyte
279 proliferation. However, in contrast to the metronidazole-nitroreductase ablation model,
280 analysis of cardiomyocyte proliferation in *irf8*$^{-/-}$ mutants revealed that they too
281 significantly increased the percentage of EdU+ cardiomyocytes following injury,
282 comparably to *irf8*$^{+/+}$ larvae (Figure 4g & 4h).
283
284 To resolve this disparity, we examined more closely the differences between these
285 models. We found, like others[18], that *irf8*$^{-/-}$ mutants possess a greater global number
286 of neutrophils than observed in *irf8*$^{+/+}$ fish and mount a larger neutrophil response to
287 injury (Supplementary Figure 5b & 5c). Since we do not observe an increased
288 neutrophil response in NTR+met+ larvae, we hypothesised that neutrophils might be
289 compensating for macrophages in *irf8*$^{-/-}$ larvae (Supplementary Figure 5d). To test this
290 hypothesis, we inhibited neutrophil recruitment in *irf8*$^{-/-}$ larvae using the receptor
291 antagonist 'SB225002' which blocks CXCR1/2 activation, a key chemokine receptor
292 for neutrophil migration. CXCR1/2 inhibition successfully lowered the number of
293 recruited neutrophils (2.0±3.4 vs 0.43±0.18) and abolished the injury-associated
294 increase in cardiomyocytes in *irf8*$^{-/-}$ (Supplementary Figure 5e-g). Taken together, this
295 suggests that macrophages are required for cardiomyocyte proliferation but can be
296 substituted by excess neutrophils.
297

298 **Regenerating larval hearts resolve inflammation and enter a reparative stage by**
299 **48 hpi**
300
301 Next, we sought to understand which biological processes might still be occurring by
302 the final 48 hpi timepoint of the larval cardiac injury model. We performed RNAseq on
303 pooled, uninjured and injured larval hearts at 48 hpi (Figure 5a). We found 418 genes
304 were upregulated (log_2 fold change >1), and 1,046 downregulated in injured hearts.
305 We did not observe differential expression of markers of proliferation such as MCM2,
306 mKi67 and PCNA, suggesting that the proliferation we observe from 24 hpi is
307 concluded by 48 hpi (Figure 5b). In agreement with this, gene ontology analysis
308 indicated categories such as growth factors and cell proliferation not to be enriched at
309 48 hpi (Supplementary Figure 6e).
310
311 Most inflammatory and M1 markers were either not differentially expressed or were
312 downregulated in injured hearts, such as Il1b (Figure 5b & Supplementary file 1). In
313 contrast, we found injury-associated upregulation of 39 collagen isoforms, several
314 profibrotic genes such as *tgfb1a* and markers of epithelial to mesenchymal transition
315 (EMT) such as *vimentin*. Similarly, hierarchical clustering of differentially expressed
316 genes revealed 9 distinct clusters with Cluster 1 being upregulated in injured hearts
317 and enriched in collagens, matrix metalloproteins (MMPs) and fibroblast growth factors
318 (FGFs) (Figure 5c, Supplementary file 2). Additionally, Cluster 2 contained several
319 EMT genes, Cluster 8 genes relating to cell recruitment and lymphangiogeneis whilst
320 Cluster 7 contained several embryonic-associated myosins and myosin binding
321 proteins such as *myl10* and *cald1b*. Clusters 3-6 & 9 were downregulated in injury,
322 Cluster 2 was enriched for immune genes and Clusters 4 and 6 for growth factors, with
323 Clusters 3 and 5 having no clear identity. Taken together, our RNAseq results suggest
324 that the inflammatory and proliferative stages are largely concluded by 48 hpi and that
325 a pro-resolving and reparative phase dominates thereafter.
326
327 **Cardiac injury induces epicardial activation and VEGFaa upregulation**
328
329 Our detailed characterisation of the larval laser injury model revealed a macrophage-
330 dependent, cardiomyocyte proliferative response occurring at 24-48 hpi. We therefore
331 utilised the rapidity and imaging opportunities offered by the model to investigate the

underlying mechanism of the induction of cardiomyocyte proliferation. Epicardial VEGFaa has recently been demonstrated to drive cell cardiomyocyte proliferation in adult zebrafish following cryoinjury and we hypothesised the same mechanism might drive cardiomyocyte proliferation in the injured larval heart[33].

We found robust *vegfaa:GFP* expression specifically in mesothelial cells overlying the myocardium (Figure 6a). Colocalisation with established epicardial marker *tcf21* in uninjured *Tg(tcf21:DsRed;vegfaa:GFP)* larvae confirmed these cells to be early epicardium (Figure 6b). Next we investigated if epicardial *vegfaa:GFP* expression changes following injury by 3D fluorescence intensity analysis of uninjured and regenerating hearts. We found that epicardial *vegfaa:GFP* intensity increased significantly at 48 hpi (Figure 6c & 6d). Interestingly, this was due both to an increase in the number of epicardial cells and their individual intensity suggesting the epicardium activates and responds to injury by both proliferation and gene expression changes to increase VEGFaa (Supplementary figure 7c & 7d).

Macrophages localise to the epicardial niche and induce the expansion of epicardial cell number

Given that our data showed that macrophage ablation abolishes injury-dependent cardiomyocyte proliferation (Figure 5f), we hypothesised that macrophages might be required for epicardial activation. To test this hypothesis, we ablated macrophages and assessed if epicardial activation still occurred at 48 hpi. Following injury we observed increased *vegfaa:GFP* expression in both macrophage-replete NTR-met+ and NTR+met- groups, but not in macrophage ablated NTR+met+ hearts (Figure 6f & 6g). Interestingly, macrophage ablation did not affect *vegfaa:GFP* expression per cell, but did block the expansion of epicardial cell number following injury (Figure 6h & Supplementary Figure 7e). Furthermore, 3D analysis of macrophage localisation following injury showed that recruited macrophages invade the myocardial-epicardial niche and synapse with epicardial cells (Figure 6e). Importantly, macrophage or neutrophil *vegfaa:GFP* expression was not observed at any timepoint (Supplementary Figure 7a & 7b). Our data therefore strongly suggest that the recruitment of macrophages to the epicardium is essential for subsequent epicardial activation, thus increasing net cardiac *vegfaa* expression.

366

367 **VEGFaa is both required and sufficient for cardiomyocyte proliferation in larval**
368 **zebrafish**

369

370 To verify if epicardial VEGFaa was driving cardiomyocyte proliferation in larval cardiac
371 regeneration, we first tested if VEGFaa was sufficient to stimulate cardiomyocyte
372 proliferation. Recombinant zebrafish VEGFaa protein (zfVEGFaa) was intravenously
373 microinjected into the circulation of 72 hpf *Tg(myl7:h2b-GFP)* larvae and total
374 cardiomyocyte number assessed at 24 and 48 hpt (hours post-treatment) (Figure 7a).
375 zfVEGFaa increased total cardiomyocyte number by 13.3% relative to PBS-injected
376 controls at 24 hpt (Figure 7b & 7c).

377

378 To test if VEGF signalling is required for injury-associated cardiomyocyte proliferation,
379 we used a high-affinity, pan-VEGFR receptor antagonist AV951 (Tivozanib) to block
380 VEGF signalling[34]. We bathed larvae in 10nM AV951 over the course of our cardiac
381 injury model, pulsed with EdU at 24-48 hpi and quantified EdU+ cardiomyocytes at 48
382 hpi (Figure 7d). Interestingly, AV951 decreased the proportion of EdU+
383 cardiomyocytes in both the uninjured and injured groups (uninjured 38.4±3.4 vs
384 28.0±3.0 and injured 42.9±3.8 vs 31.6±2.2, n=13-36) (Figure 7e & 7f). Together, these
385 data suggest that VEGF signalling in the heart is driving cardiomyocyte proliferation in
386 the larval heart, both as part of normal development and following cardiac injury.

387

388 **Notch and Nrg-ErbB signalling are required for cardiomyocyte proliferation**

389

390 We next investigated if macrophage-induced epicardial VEGFaa signalling could be
391 interacting with more established effectors of cardiomyocyte proliferation. Notch and
392 Nrg-ErbB were strong candidates as both are required for adult heart regeneration
393 and cardiomyocyte proliferation in adult zebrafish[35–38]. We first verified if these
394 signalling pathways were required for cardiomyocyte proliferation in the larval heart
395 following injury. We laser-injured *Tg(myl7:nlsDsRed)* larvae, and bathed them in
396 100μM of pan-notch inhibitor DAPT ((N-[N-(3,5-difluorophenacetyl)-l-alanyl]-S-
397 phenylglycine t-butyl ester) (Figure 7g). DAPT is a gamma secretase inhibitor and has
398 been demonstrated in both zebrafish and drosophila to phenocopy notch mutants[39–

399 [41]. Notch signalling inhibition decreased cardiomyocyte number by ~8% in uninjured
400 hearts (253.3±5.2 vs 233.4±4.5, n=25-38) and ~14% injured hearts (266.0±5.6 vs
401 229.5±3.6, n=25-38). (Figure 7h & 7i).
402
403 We repeated this experiment, with 1.75μM ErbB2 antagonist AG1478 (Figure 7g).
404 Small molecule inhibitor AG1478 selectively inhibits ErbB2, a required co-receptor for
405 ErbB4 dimerization and subsequent neuregulin signal transduction and faithfully
406 phenocopies *erbb2* mutants[42]. Interestingly, the results exactly replicated those of the
407 notch signalling inhibition experiment, decreasing cardiomyocyte number by ~9% in
408 uninjured (257.2±5.8 vs 235.2±4.2) and by ~13% in injured hearts (265.7±5.5 vs
409 229.5±5.9) (Figure 7j & 7k). These results confirm that both notch signalling and Nrg-
410 ErbB signalling are required for the expansion of cardiomyocyte number in both
411 uninjured and injured larval hearts.
412
413 **Cardiac injury and VEGFaa induce endocardial notch signalling**
414
415 Given the individual requirement of VEGF, notch and Nrg-ErbB signalling for
416 cardiomyocyte proliferation in the larval heart, we sought to understand if these
417 signalling components might act in one pathway. Previous studies have demonstrated
418 developmental larval zebrafish heart growth to be activated by cardiac contraction, via
419 endocardial-notch>Nrg-ErbB signalling[43,44]. We hypothesised that VEGFaa might be
420 driving cardiomyocyte proliferation by increasing endocardial notch signalling and
421 consequently augmenting this developmental pathway (Figure 8a).
422
423 To test if VEGFaa could activate endocardial notch signalling, we utilised the notch
424 signalling reporter line *Tg(Tp1:venus-PEST)* as a readout of cardiac notch signalling.
425 Recombinant zfVEGFaa injected into 3 dpf larvae, and their hearts were analysed *via*
426 heart-synchronised light-sheet microscopy at 6, 24 and 48 hpt (Figure 8b).
427 Furthermore, an additional group of larvae were injected with zfVEGFaa but also
428 bathed in ErbB2 antagonist AG1478. According to our hypothesised pathway (Figure
429 8a), we reasoned that zfVEGFaa injection should upregulate notch signalling but that
430 inhibition of Nrg-ErbB signalling should be unable to suppress zfVEGFaa-induced
431 notch upregulation.

432

433 Notch signalling was primarily in the endocardium, colocalising with endothelial
434 reporter *kdrl:mCherry* but was relatively low intensity and only detectable in a subset
435 of larvae at any given timepoint (Figure 8c). We found, zfVEGFaa injection increased
436 the percentage of larvae with notch+ (Tp1:Venus+) endocardium (46.4% to 78.6%,
437 n=28) at 6 hpi but not at the 24 and 48 hpi timepoints (Figure 8d). Furthermore,
438 AG1478 failed to block the increase in the percentage of notch+ hearts following
439 zfVEGFaa injection, confirming Nrg-ErbB signalling was not upstream of *vegfaa* or
440 notch signalling. In fact, zfVEGFaa+AG1478 treated larvae had a substantially higher
441 percentage of notch+ hearts at 48 hpi than those treated with zfVEGFaa alone (25.0%
442 vs 0%). This is suggestive of a negative feedback mechanism, supporting previous
443 findings of Nrg-ErbB being downstream of notch signalling[43].
444

445 To test if this pathway (Figure 8a) acted similarly in injury, we substituted zfVEGFaa
446 injection for cardiac injury and repeated the experiment (Figure 8e). Cardiac injury
447 similarly increased the percentage of hearts possessing notch+ endocardium but this
448 occurred later, at 48 hpi (50.0% vs 11.1%, n=18) (Figure 8f & 8g). As before, AG1478
449 did not block notch signalling, rather it seemed to enhance it. Whilst the percentage of
450 notch+ hearts in the injured group did not significantly increase by 24 hpi,
451 injured+AG1478 treated larvae did significantly increase relative to uninjured larvae
452 (52.9% vs 11.1%).
453

454 Taken together, these results demonstrate that cardiac injury and VEGFaa increase
455 endocardial notch signalling, providing a novel mechanism whereby macrophages can
456 trigger cardiomyocyte proliferation via stimulation of epicardial *vegfaa* expression.
457

458 **Discussion**

459

460 In this study we have presented the first detailed characterisation of the larval
461 zebrafish model of heart regeneration, demonstrating the heterogeneity and plasticity
462 of macrophages in cardiac injury and testing the requirement of macrophages for the
463 removal of apoptotic cells, cardiomyocyte proliferation, epicardial activation and
464 recovery of cardiac structure and function. Furthermore, we demonstrated the utility of
465 the larval cardiac injury model by taking advantage of its *in vivo* cardiac imaging

466 opportunities and amenability to pharmacological intervention to discover a novel role
467 for macrophages in driving cardiomyocyte proliferation via epicardial activation.
468
469 Our examination of macrophages in larval zebrafish cardiac injury suggests that they
470 may faithfully recapitulate the phenotypic complexity and function found in the adult
471 cryoinjury model. As previously shown in adult hearts[29], we detected mpeg1+csf1ra+
472 and mpeg1+csf1ra- macrophage subsets. We found these cells to have identical
473 recruitment dynamics and no obvious differences in morphology or behaviour. Recent
474 Cre-Lox lineage tracing has shown that mpeg1+csf1ra- cells have a non-
475 haematopoietic origin, are csfr1a-independent developmentally and, unlike
476 mpeg1+csf1ra+ cells, are not phagocytic[45,46]. Future work should focus on
477 understanding the precise roles of these subsets in cardiac regeneration, in particular
478 mpeg1+csf1ra- macrophages.
479
480 In addition to macrophage heterogeneity, we observed macrophage phenotypic
481 plasticity. We used heartbeat-synchronised live imaging to show that macrophages
482 can convert from mpeg1+tnfa- to mpeg1+tnfa+. This is the first time that macrophage
483 phenotype conversion has been imaged in the heart. Studies examining zebrafish
484 macrophages in spinal cord and tail transection have demonstrated *tnfa* to mark M1-
485 like macrophages, which then transition to M2-like macrophages[24]. Our success in
486 increasing the percentage of tnfa+ macrophages by canonical M1-polarising cytokine
487 IFN-γ-rel suggests that early tnfa+ macrophages are indeed proinflammatory. In
488 agreement with findings in the in the adult cryoinjured heart[29], we found this tnfa+
489 population of macrophages to be transient, only observed in the early response at 24
490 hpi. Similarly, our RNAseq data showed that, by 48 hpi, injured larval hearts
491 downregulate inflammatory cytokines and growth factors but upregulate collagens and
492 reparative cytokines. Our finding that a pro-resolving, fibrotic program is activated in
493 injured hearts, despite full structural and functional recovery, is in agreement with a
494 recent study showing the scar-deficient runx1$^{-/-}$ zebrafish to undergo successful
495 cardiac regeneration[47]. It might be that the fibrotic program is concomitantly activated
496 upon resolution of inflammation, irrespective of a requirement for scar tissue.
497
498 We used two separate methods to examine the role of macrophages in larval heart
499 regeneration. Interestingly, ablation via csf1ra-driven nitroreductase expression was

500 still able to abolish numbers of csf1ra- macrophages at the injured heart. Possibly this
501 is indicative of a positive-feedback system where csf1ra- macrophage recruitment is
502 dependent on csf1ra+ macrophages. Cell death data acquired by either technique
503 demonstrated that macrophages are required for the timely removal of apoptotic cells
504 following injury. Interestingly, these apoptotic cells do eventually seem to be cleared
505 even in the absence of macrophages. Our live imaging showed that dead
506 cardiomyocytes can be expelled from the myocardium independently of macrophages.
507 It is possible that this is a mechanical consequence of cardiac contraction, although a
508 similar phenomenon is known to occur in neuroepithelium where neurons appear to
509 extrude apoptotic cells out of tissue[48].
510
511 Surprisingly, we found that the absence of macrophages did not affect the structural
512 or functional recovery of the injured larval heart, despite macrophages being required
513 for cardiomyocyte proliferation. This is in contrast to past studies where liposomal
514 clodronate macrophage ablation and CCR2-antagonist inhibition of macrophage
515 recruitment in regenerative neonatal mice, adult zebrafish and axolotl hearts causes
516 blocked or delayed resolution of the infarct area[15,16,49]. The contrasting results in the
517 larval heart might simply be a consequence of its small size and low transmural
518 pressure, allowing surviving myocardium to rapidly 'knit' back together. Supporting
519 this, we observed individual cardiomyocytes extending protrusions into the lesion.
520 Previous histological analysis of the border zone in injured adult zebrafish and
521 neonatal mouse hearts has shown cardiomyocytes exhibiting a similar mesenchymal
522 phenotype following partial dedifferentiation and disassembly of sarcomeres[50,51].
523 However, this is the first time this behaviour has been verified by time-lapse imaging
524 live in a beating heart.
525
526 Studies in adult zebrafish and neonatal mice have shown ablation of macrophages to
527 decrease cardiomyocyte proliferation[15,17]. However, early revascularisation is critical
528 for cardiomyocyte proliferation and is macrophage-dependent, calling into question
529 whether macrophages directly induce cardiomyocyte proliferation[17,52]. Larval hearts
530 do not have supporting vasculature[26]; therefore our finding that cardiomyocyte
531 proliferation is macrophage-dependent suggests macrophages facilitate
532 cardiomyocyte proliferation by means other than revascularisation. Indeed, our data
533 indicate a novel mechanism whereby macrophages are recruited to the epicardial-

534 myocardial niche and induce expansion of epicardial cell numbers and increase in the
535 expression of mitogenic VEGFaa. This might explain previous findings in developing
536 and injured mouse hearts where yolk-derived and Gata6+ pericardial cavity
537 macrophages are recruited to the epicardium, respectively[53,54] Future studies should
538 seek to identify precisely how macrophages activate epicardium. Given we found that
539 neutrophils can compensate for macrophages for cardiomyocyte proliferation, it is
540 possible that a shared inflammatory factor triggers epicardial activation.
541
542 Endocardial notch signalling is required for cardiomyocyte proliferation in cryoinjured
543 adults and myocardial growth by downstream Nrg1 in larvae[43,55,56]. Therefore, our
544 finding that injury and VEGFaa increase endocardial notch signalling reveals an
545 important mechanism whereby the epicardium can induce cardiomyocyte proliferation.
546 In agreement with previous studies, we showed both notch and Nrg-ErbB signalling to
547 be required for expansion of cardiomyocyte numbers in both uninjured and injured
548 hearts[57–59]. Since we found VEGFaa inhibition decreased cardiomyocyte proliferation
549 in uninjured larval hearts, it is likely that VEGFaa>notch>Nrg-ErbB is a developmental
550 cardiac growth pathway that is upregulated upon injury and thus might be conserved
551 in mammals. Our discovery that macrophages act upstream of this pathway therefore
552 opens up exciting immunomodulatory opportunities for therapeutic enhancement of
553 cardiac repair in the future.
554
555 **Materials and Methods**
556
557 **Zebrafish husbandry and lines used**
558
559 Zebrafish husbandry and maintenance was conducted as per standard operating
560 procedures, in accordance with the Animals (Scientific Procedures) Act, 1986 and
561 approved by The University of Edinburgh Animal Welfare and Ethical Review Board in
562 a United Kingdom Home Office-approved establishment. All our experiments were
563 performed on staged zebrafish aged between 3 dpf and 5 dpf. The following transgenic
564 and mutant lines were used: *Tg(myl7:eGFP)*^{twu26} [60], *Tg(mpx:mCherry)*^{uwm7} [61],
565 *Tg(mpeg1:mCherry)*^{gl23} [62], *Tg(mpeg1:eGFP)*^{gl22} [62], (*Tg(mpx:GFP)* ^{i114} [63], *Tg(myl7:h2b-*
566 *GFP)*^{zf52} [64], *Tg(myl7:mKateCAAX)*^{SD11} [65], *Tg(fms:Gal4.VP16)*^{i186}*,* referred to as
567 csfr1a:gal4[66], *Tg(UAS-E1b:NfsB-mCherry)*^{c264} abbreviated to UAS:NfsB-mCherry[67]*,*

568 *Tg(vegfaa:eGFP)*^{PD260} [33], *Tg(myl7:nlsDsRed)*^{f2} [68] *Tg(TNFa:eGFP)*^{sa43296} [24],
569 *Tg(Tp1:venus-PEST)*^{S940} [69], *Tg(kdrl:hsa.HRAS-mCherry)*^{S896} [70], *Tg(kdrl:GFP)*^{la116} [71],
570 *Tg(tcf21:DsRed)*^{PD37} [72], *Tg(myl7:gal4:myl7:GFP)*^{cbg2Tg} [73] and irf8$^{st95/st95}$ [27] referred to as
571 *irf8*$^{-/-}$. *Tg(csf1ra:gal4:UAS:NfsB-mCherry)* is abbreviated to csf1ra:NfsB-mCherry
572 throughout the manuscript for simplicity. Adults were day-crossed as appropriate to
573 yield desired combinations of transgenes in embryos. Embryos were treated with
574 0.003% phenylthiourea (Fisher Scientific) at 7 hpf to prevent pigment formation and
575 therefore enhance image clarity. Embryos and larvae were incubated at 28.5°C in
576 conditioned media/water (6.4 mM KCl, 0.22 mM NaCl, 0.33 mM $CaCl_2 \cdot 2H_2O$, 0.33 mM
577 $MgSO4 \cdot 7H_2O$) + 0.1% methylene blue (w/v) and imaged at room temperature (23°C)
578 using epifluorescence or light sheet fluorescence microscopy (details below). When
579 necessary, larvae were anesthetized using 40 µg/ml tricaine methanesulfonate (Sigma
580 Aldrich) in conditioned media.
581
582 **Cardiac laser injury**
583
584 A Zeiss Photo Activated Laser Microdissection (PALM) laser system (Zeiss) was used
585 to precisely cause a localised injury at the ventricular apex of anesthetized 72 hpf
586 larvae[26]. Larvae were mounted on a glass slide in 20 µl anesthetized conditioned
587 media and lasered via a 20X objective. Injuries were deemed successful and complete
588 once ventricular contractility decreased, the apex had shrunk, and the myocardial wall
589 had swollen without causing cardiac rupture and subsequent bleeding. A successful
590 cardiac injury results in the portion of dysfunctional tissue losing fluorescent
591 myocardial transgenic fluorescence signal. Uninjured larvae were treated in the same
592 manner up to the point of laser injury, when they were individually transferred into
593 single wells of a 24-well plate and maintained in the same environmental conditions
594 as injured fish.
595
596 **Epifluorescence microscopy**
597
598 Larvae were mounted laterally in conditioned media on a glass slide and imaged using
599 a Leica M205 FA stereomicroscope with GFP and mCherry filters. For all serial
600 timepoint epifluorescence imaging experiments, number of immune cells on the heart

601 were quantified by manually observing and counting cells moving synchronously with
602 the beating heart. Heart images were acquired using 2X 0.35NA objective.
603
604 **Heart-synchronised light-sheet microscopy**
605
606 Individual larvae were prepared for light sheet fluorescence microscopy (LSFM) by
607 embedding in 1% low melting-point agarose (ThermoFisher) in anesthetized
608 conditioned media inside FEP tubes (Adtech Polymer Engineering). Agar embedding
609 prevents gradual drift of the embryo in the FEP tube, without causing developmental
610 perturbations during long-term imaging. Larvae were used only once for a time-lapse
611 imaging experiment, and any repeats shown come from distinct individuals. Larvae
612 were mounted head down such that the heart faces toward both illumination and
613 imaging objectives to improve image clarity. All LSFM experiments were performed at
614 room temperature (23°C). Camera exposure times ranged from 5-15 ms, laser
615 excitation power was 11mW and scans were performed at 3-5 minute intervals.
616 Brightfield images acquired at 80 fps were analysed in real-time to enable optically-
617 gated acquisition of fluorescence z slices at a set phase of cardiac contraction, usually
618 mid diastole. The setup of our custom-built LSFM system has been previously reported
619 in detail[30].
620
621 **Metronidazole-nitroreductase macrophage ablation model**
622
623 In order to selectively ablate macrophages prior to cardiac injury, embryos were
624 incubated as previously described until 48 hpf and then treated as follows. Embryos
625 were carefully dechorionated at 48 hpf and screened based on fluorescence and split
626 into groups appropriate to the experiment, for example larvae were always split into
627 csf1ra:gal4;UAS:NfsB-mCherry+ and csf1ra:gal4;UAS:NfsB-mCherry-. Embryos were
628 then transferred to either conditioned water or a 0.5mM metronidazole (Thermo Fisher
629 Scientific) solution, both solutions also contained 0.003% phenylthiourea (Thermo
630 Fisher Scientific) and 0.2% DMSO (Sigma Aldrich). Larvae were then incubated in
631 these solutions in the dark at 28. 5°C for 24 hours prior to injury at 72 hpf. Larvae were
632 then removed from the metronidazole solution and vehicle solution and placed in fresh
633 conditioned water + 0.003% phenylthiourea for the remainder of the experiment. As

634 shown in Figure 2, this is sufficient to ablate macrophages prior to injury and
635 completely block subsequent macrophage recruitment to the injured heart.
636
637 **Neutral red staining**
638
639 Larvae were incubated at 72 hpf in 5μg/mL neutral red in conditioned water for 5 hours
640 in the dark at 28.5°C. Larvae were then washed twice for 5 minutes in conditioned
641 water, anaesthetised with 40 µg/ml tricaine methanesulfonate and imaged by
642 brightfield microscopy on a Leica M205 FA stereomicroscope.
643
644 **Genotyping of *irf8*$^{-/-}$ mutants**
645
646 Adult (>30 dpf) zebrafish arising from heterozygous *irf8* mutant incrosses were
647 anaesthetised in 40 µg/ml tricaine methanesulfonate and a lobe of caudal fin removed
648 by scalpel. After clipping, fins were digested to extract DNA using 10mg/ml Prot K,
649 incubated at 65oC for 1 hour. This incubation ends with 15 minutes at 95ºC to denature
650 the Proteinase K. A section of irf8 flanking the mutation locus was then amplified from
651 the extracted DNA by PCR using Forward -ACATAAGGCGTAGAGATTGGACG and
652 Reverse -GAAACATAGTGCGGTCCTCATCC primers and REDTaq® ReadyMix™
653 PCR Reaction Mix. The PCR product was then digested for 30 minutes at 37 ºC using
654 AVA1 restriction enzyme (New England Bioscience) and the product run on a 2%
655 agarose gel. WT = AvaI digest site is present = PCR product is cleaved to give two
656 bands with sizes of approximately 200 and 100 bp. irf8 $^{-/-}$ = AvaI digest site is absent
657 due to mutation = PCR product is not cut. A single band is observed with a size of 286
658 bp. irf8 $^{+/-}$ = Three bands as above.
659
660 **Microinjection recombinant proteins and intravital stains**
661
662 Microinjections were performed on larvae at 72 hpf using a Narishige IM-300
663 Microinjector and pulled thin wall glass capillaries (Harvard Apparatus), administered
664 under anaesthesia by intravenous microinjection through the cardiac sinus venosus
665 (SV) that drains the common cardinal vein (CCV). An injection volume of 1 nL was
666 used for all intravenous injections to minimise disruption to blood volume.
667

668 For propidium iodide intravital staining, 1nL 100µg/ml propidium iodide in DPBS was
669 injected immediately following injury at 0.5 hpi. Larvae were then immediately imaged
670 by heartbeat-synchronised light-sheet microscopy at 1 hpi. Injection of recombinant
671 zfIFN-γ-rel (IFN-1.1) (Kingfisher Bioscience) was administered as a single 1nL 132nM
672 dose at 72 hpf. Lyophilised IFN- γ-rel was reconstituted in PBS + 0.1% BSA (carrier
673 protein) and PBS + 0.1% BSA was used as the vehicle control solution. Injections of
674 recombinant zfVEGFaa (Kingfisher Bioscience) were administered as single 1nL 0.25
675 ug/ul doses at 72 hpf (protein reconstituted as above).
676
677 **Histological staining**
678
679 To detect cell death at the injured ventricle, whole-mount larval TUNEL staining was
680 performed. Larvae were fixed in 4% PFA for 30 minutes and transferred to 1:10 dilution
681 of PBS. Larvae were subsequently digested in 1 µg/ml Proteinase K for 1 hour. Larvae
682 were re-fixed in 4% PFA for 20 minutes and subsequently washed in PBT. TUNEL
683 staining was performed using ApopTag Red In situ kit (MilliporeSigma) to label
684 apoptotic cells, as described previously[26]. Stained hearts were imaged using LSFM.
685
686 EdU staining was performed by incubating larvae in 1 mM EdU (5-ethynyl-2′-
687 deoxyuridine) (Abcam) in 1 % DMSO (Sigma Aldrich) in conditioned water + 0.003%
688 phenylthiourea (Thermo Fisher Scientific) for 24 hours beginning either at 0 hpi or 24
689 hpi depending on the experiment. Larvae were incubated at 28.5°C in the dark. Larvae
690 were then fixed for 2 hours at room temperature in 4% PFA, permeabilised in
691 permeabilisation solution (PBS-Triton-X 0.1% + 1% Tween + 1% DMSO) and
692 pericardium punctured using a glass microinjection needle (further improving
693 permeability). Larvae were then washed twice in PBS-3% BSA and incubated for 2
694 hours at room temperature in CLICK reaction mixture from Click-iT™ EdU Imaging Kit
695 with Alexa Fluor™ 594 (Invitrogen) made according to manufacturers' instructions.
696 Larvae were finally washed once in PBS-3%BSA and twice in PBS-0.1% tween and
697 imaged by LSFM.
698
699 **Heart lesion size quantification**
700

701 Larval hearts expressing the transgene *myl7:GFP* were imaged by heartbeat-
702 synchronised light-sheet imaging as described above. Exposure was kept consistent
703 at 10ms, along with z slice spacing (1 μm), and heart contraction phase was locked to
704 mid diastole for all larvae. Z stacks were surface rendered in IMARIS (Bitplane) based
705 on absolute intensity, and software-suggested segmentation and rendering
706 parameters. Lesion area, visualised as a render-free hole in the myocardium, was then
707 traced around manually and lesion area quantified in FIJI (National Institutes of
708 Health)[74].
709
710 **Ventricular ejection fraction analysis**
711
712 Larval hearts of *Tg(myl7:GFP)* larvae were imaged at 80 fps in brightfield using a Leica
713 M205 FA epifluorescence stereomicroscope, to capture when the ventricle was in
714 diastole and systole. The ventricular area in diastole and systole was measured
715 manually in FIJI and ventricular ejection fraction calculated using the formula 100 X
716 [(Diastolic Area – Systolic Area)/Diastolic Area][25]. Ventricular ejection fraction by area
717 was then converted to ejection fraction by volume using the formula 'Ejection fraction
718 by area x 2.33 = Ejection fraction by volume' derived in Supplementary Figure 4. Over
719 the small range of ejection fractions that occur in larval hearts, the relationship can be
720 considered to approximate to a linear one.
721
722 **Quantification of cell number by image analysis**
723
724 To quantify the number of cardiomyocytes in *Tg(myl7:h2b-GFP)* and
725 *Tg(myl7:nlsDsRed)* larval hearts, z stacks of hearts acquired by LSFM were imported
726 into FIJI and nuclei counted using the plugin Trackmate. Briefly, key segmentation
727 parameters 'Estimated blob diameter'=5.5, 'Threshold'=0.9 were taken as a starting
728 point, and optimised manually per experiment until all nuclei are counted successfully.
729 The heart atrium is excluded manually by x coordinate filtering and ventricular
730 cardiomyocytes are then automatically counted by the plug in.
731
732 In order to automatically quantify the percentage of EdU+ ventricular cardiomyocytes
733 in *Tg(myl7:h2b-GFP)* larval hearts, a custom FIJI macro was written to exclude non-
734 cardiomyocyte EdU signal. This is necessary as cardiomyocytes have a much lower

735 turnover rate than surrounding cells in the pericardium, endocardium and blood and
736 so represent a minority of EdU+ cells. Briefly, the Bersen segmentation method was
737 used to mask areas of GFP fluorescence per z slice and these masks subsequently
738 applied as a crop RoI to EdU signal in the 641 nm colour channel of RGB images.
739 Slices were then reassembled and merged into maximum intensity projections, where
740 the FIJI[74] Trackmate plugin was used to count both the total number of GFP+
741 cardiomyocyte nuclei and EdU+ cardiomyocyte nuclei. This quantification then allowed
742 the percentage of EdU+ cardiomycytes to be calculated in an unbiased way per larval
743 heart.
744
745
746 **Quantification of notch signalling by image analysis**
747
748 In order to objectively identify whether the hearts from *Tg(Tp1:venus-PEST)* larvae
749 possessed venus signal in the endocardium above that of background, and were
750 therefore 'notch+', the following approach was used. Treatment groups were blinded
751 to the analyser, and z stacks opened in FIJI. The automatic brightness and contrast
752 function was used to objectively enhance the signal in the heart, and the clear interface
753 between the granular autofluorescence of the chamber blood and the smooth
754 autofluorescence of the myocardium searched for venus expression. The distinctive
755 morphology and location of endothelium allowed for unambiguous identification of
756 venus+ status.
757
758 **Pharmacological inhibition of larval signalling**
759
760 To inhibit VEGF signalling, larvae were bathed in pan-VEGFR antagonist
761 AV951/Tivozanib (Stratech Scientific) 0-48 hpi. AV951 was dissolved in 0.1% DMSO
762 in conditioned water + 0.003% phenylthiourea to make a 10 nM solution, with just 0.1%
763 DMSO in conditioned water + 0.003% phenylthiourea becoming the vehicle control. In
764 order to pulse larvae with EdU, the original solution was replaced fresh solution, with
765 the addition of 1mM EdU at 1% DMSO.
766
767 To inhibit notch signalling, larvae were bathed in gamma secretase inhibitor DAPT
768 (Cambridge Bioscience) 0-48 hpi. DAPT was dissolved in 0.2% DMSO in conditioned

769 water + 0.003% phenylthiourea to make a 100μM solution, with just 0.2% DMSO in
770 conditioned water + 0.003% phenylthiourea becoming the vehicle control. Note, DAPT
771 must be dissolved in DMSO prior to the addition of water to prevent precipitation.
772
773 In order to inhibit neuregulin-ERBB signalling, the ErBB2 antagonist AG1478 was
774 used. Larvae were bathed in 1.75 μM AG1478 (Cambridge Bioscience) dissolved in
775 0.25% DMSO in conditioned water + 0.003% phenylthiourea over 0-48 hpi.
776
777 **Extraction of larval hearts and RNA extraction**
778
779 Following laser injury at 72 hpf *Tg(myl7:gal4::GFP;UAS:mRFP)* larvae were incubated
780 at 28.5°C in conditioned media/water + 0.1% methylene blue (w/v) + 0.003%
781 phenylthiourea. At 48 hpi uninjured and injured larvae were given an overdose of
782 tricaine at 400 μg/ml, following which hearts were extracted. We adapted the protocol
783 of Burns and MacRae[75] to increase the yield of heart retrieval from ~50% to ~70%.
784 Briefly, ~30 larvae were placed in 2mL eppendorf tubes, the conditioned water drained
785 and replaced with ice cold Leibovitz's L-15 Medium supplemented with 10% FCS. A
786 19-gauge needle coupled to a 5mL syringe was used to shear the larvae by aspiration
787 and therefore dissociate hearts from the rest of the larva. The lysate was then
788 inspected by epifluorescence microscopy and mRFP+ hearts and collected to be kept
789 on ice. Hearts were then digested at for 10 minutes at 4°C in protease solution (5 mM
790 CaCl2,10 mg/ml B. Licheniformis protease, 125 U/mL DNase I in 1x PBS) with
791 occasional aspiration to aid digestion, RNA was then extracted using a RNeasy Plus
792 Micro Kit (Qiagen) following direct lysis with RLT lysis buffer according to
793 manufacturer's instructions. RNA concentration was measured by Qubit and integrity
794 by Bioanalyser. RIN score for all samples ranged between 9.6-10.
795
796 **RNAseq analysis**
797
798 RNA was sequenced by Genewiz, Leipzig, Germany using Illumina NovaSeq, PE
799 2x150. Genewiz also used deseq2 package in R to evaluate sequencing quality, trim
800 reads, map to the *Danio rerio* genome and generate gene counts/hits. Sequence reads
801 were trimmed using Trimmomatic v.0.36. The trimmed reads were mapped to the
802 *Danio rerio* GRCz10.89 reference genome available on ENSEMBL using the STAR

803 aligner v.2.5.2b. Unique gene hit counts were calculated by using featureCounts from
804 the Subread package v.1.5.2. Only unique reads that fell within exon regions were
805 counted. The Wald test was used to generate p-values and log2 fold changes. A gene
806 ontology analysis was performed on the statistically significant set of genes by
807 implementing the software GeneSCF v.1.1-p2. The zfin GO list was used to cluster
808 the set of genes based on their biological processes and determine their statistical
809 significance. The volcano plot was generated by a custom R script and heatmap
810 constructed using the pHeatmap package. For the heatmap z scaled log2(Reads)
811 were clustered via Pearson correlation and clusters thresholded based on the resulting
812 dendrogram. The heatmap was generated using the pHeatmap function in R.
813
814 **Statistics**
815
816 Graphs and statistics were curated in GraphPad Prism 9.1 software (GraphPad
817 Software). Data were analysed by student *t*-test, one-way ANOVA or two-way ANOVA
818 followed by an appropriate multiple comparison *post hoc* test. All statistical tests, *p*-
819 values and *n* numbers used are given in figure legends, $p<0.05$ was deemed
820 significant in all experiments.
821
822 **Acknowledgments**
823
824 This work was funded by a British Heart Foundation (BHF) CoRE award
825 (RE/13/3/30183), Medical Research Scotland studentship (PhD-1049-2016), NC3R
826 studentship (NC/P002196/1), BHF New Horizons grant (NH/14/2/31074), and a
827 Medical Research Council UK award (MR/K013386/1). Bioinformatics and RNAseq
828 performed by Genewiz, Leipzig, Germany. We also acknowledge Amelia Edmondson-
829 Stait, University of Edinburgh, for her advice and input on RNAseq analysis.
830
831 **Author Contributions**
832
833 FAB conceived of and designed the study. FAB, AK and GM carried out all
834 experiments. Image analysis was performed by FB and AK. LSFM-related technical
835 contributions were provided by JMT. FAB wrote the manuscript. KRS, MEMO, EGS
836 and MB provided expertise regarding all RNA work. KRS helped optimise larval heart

extraction and RNA extraction. JMT, CST, MEMO, JJM, GM, MB, AGR, and MAD edited the manuscript. MAD, AGR, and CST supervised the study. All authors contributed to the article and approved the submitted version.

Figures

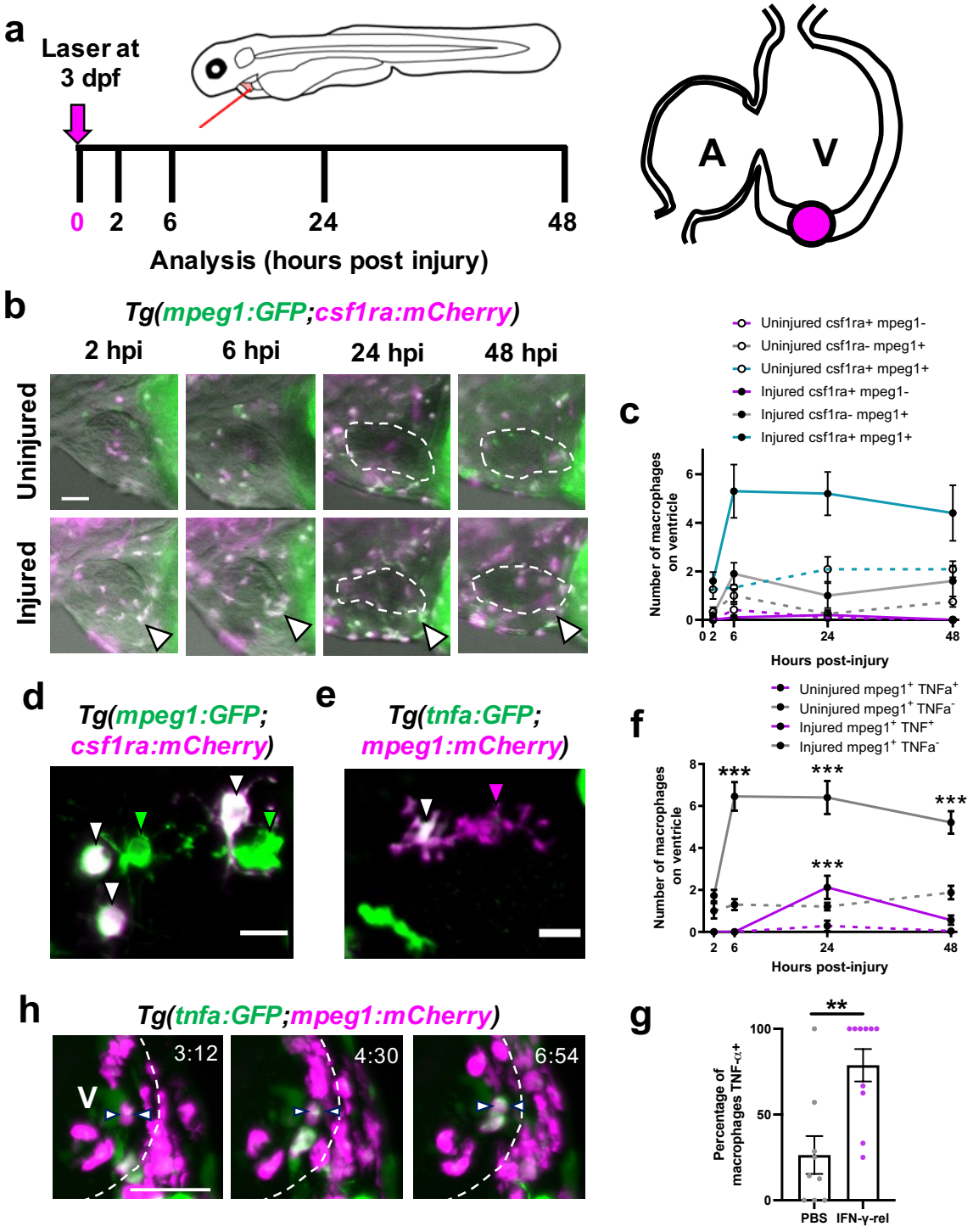

844 **Figure 1: Cardiac macrophages display heterogeneity and plasticity following**
845 **injury.**
846 (a) Schematic illustrating the cardiac laser injury model, with imaging timepoints
847 marked (left) and the injury site at ventricular apex of a 3 dpf larval heart marked
848 (magenta circle) (right). (b) Representative lateral view epifluorescence images of
849 uninjured and injured hearts at the standard timepoints in
850 *Tg(mpeg1:GFP;csf1ra:gal4:UAS:NfsB-mCherry)* (abbreviated to
851 mpeg1:GFP;csf1ra:mCherry in all panels) illustrating macrophage heterogeneity,
852 white arrow = ventricular apex; dashed line = heart outline. (c) Quantification of the
853 number of csf1ra+mpeg1-, csf1ra-mpeg1+ and csf1ra+mpeg1+ macrophages on the
854 ventricle in uninjured and injured larvae at standard timepoints, n=10-12. (d)
855 Representative LSFM image of csf1ra-mpeg1+ and csf1ra+mpeg1+ macrophages of
856 different morphologies. (e) Representative LSFM image of tnfa+mpeg1+ and tnfa-
857 mpeg1+ macrophages. (f) Quantification of number of tnfa+mpeg1+ and tnfa-mpeg1+
858 macrophages on the ventricle in uninjured and injured larvae at standard timepoints,
859 n=10-25. (g) Time-lapse timepoints for injured *Tg(tnfa:GFP;mpeg1:mCherry)*
860 ventricles imaged live in the larvae by heartbeat-synchronised LSFM microscopy
861 illustrating macrophage plasticity. Timestamps indicated, dashed line = ventricle
862 outline; arrows = macrophage converting to tnfa+. (h) Quantification of the percentage
863 of tnfa+ macrophages at 24 hpi following injection with IFN-γ-rel or PBS, n=10. Scale
864 bar = 50μm (b & h), 10μm (d & e). ***p≤0.01, ****p≤0.001*, (c & f) 2way ANOVA followed
865 by Holm-Sidak's Post-hoc test and (g) ttest.
866

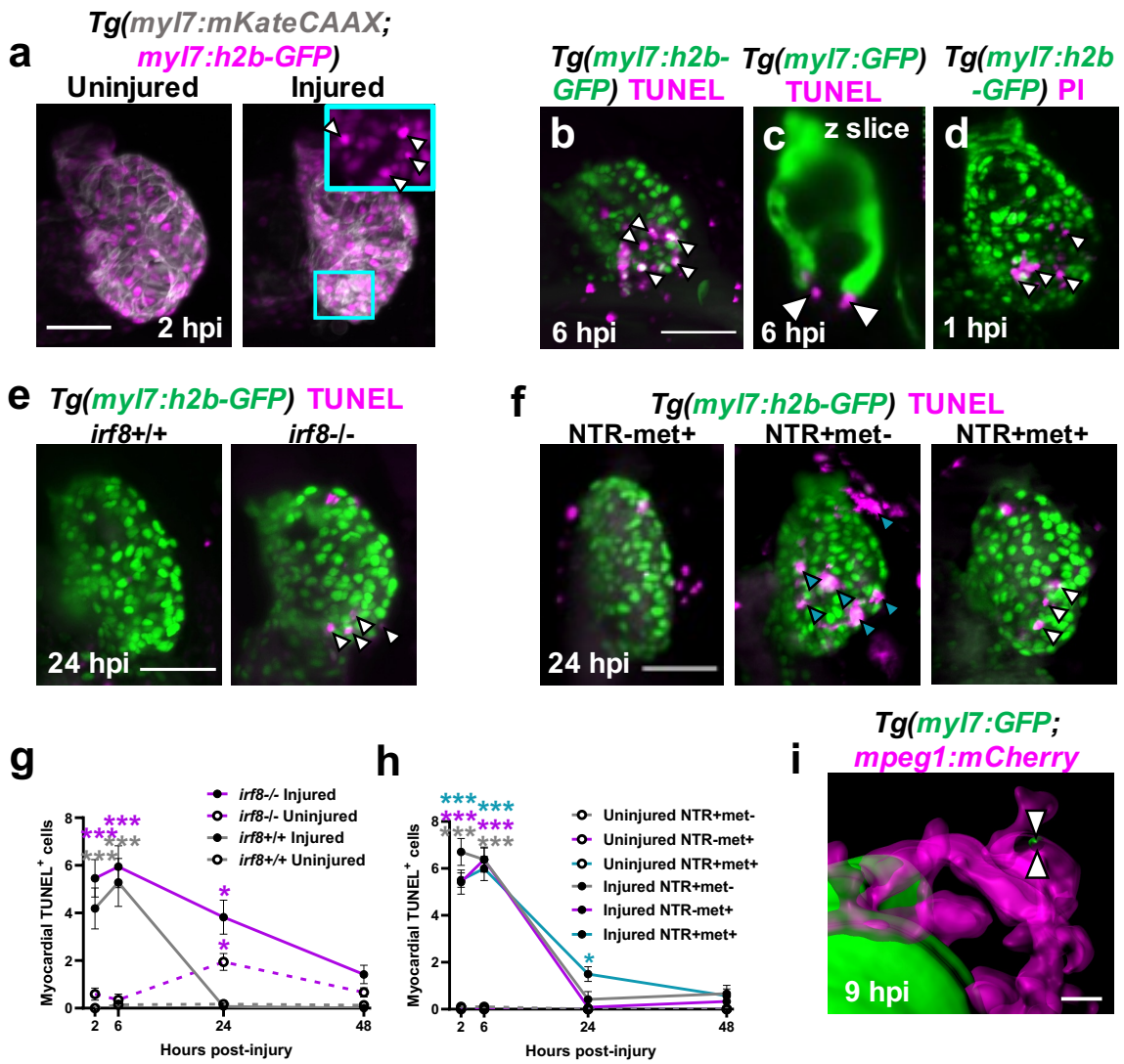

867

868 **Figure 2: Macrophages are required for timely removal of apoptotic**
869 **cardiomyocytes.**

870 (a) Representative LSFM images of uninjured and injured *Tg(myl7:h2b-*
871 *GFP;myl7:mKateCAAX)* ventricles. Cyan outlined zoom panel highlights condensed
872 nuclei (white arrowheads). Representative LSFM images of TUNEL stained hearts 6
873 hpi in (b) *Tg(myl7:h2b-GFP)* and (c) *Tg(myl7:GFP)* larvae. White arrowheads =
874 apoptotic cardiomyocytes/myocardium. (d) Representative LSFM image of a
875 propidium iodide (PI) stained *Tg(myl7:h2b-GFP)* heart at 1 hpi. White arrowheads =
876 necrotic debris. (e) Representative LSFM images of *irf8*$^{+/+}$ and *irf8*$^{-/-}$ *Tg(myl7:h2b-GFP)*
877 hearts stained by TUNEL at 24 hpi. White arrowheads = TUNEL+ cells. (f)
878 Representative LSFM images of injured *Tg(myl7:h2b-GFP;csfr1a:NfsB-mCherry)*
879 ventricles per macrophage ablation model injury group at 24 hpi. Cyan arrowheads =
880 Macrophages and white arrowheads = TUNEL+ cells. (g) Quantification of TUNEL+

881 myocardial cells in uninjured and injured, *irf8*$^{+/+}$ and *irf8*$^{-/-}$ *Tg(myl7:h2b-GFP)* ventricles,
882 n=15-29. (h) Quantification of TUNEL+ myocardial cells in uninjured and injured
883 *Tg(myl7:h2b-GFP;csfr1a:NfsB-mCherry)* ventricles per macrophage ablation group,
884 n=10-12. (i) Surface render of LSFM-acquired z stack, surfaced-rendered with 50 %
885 transparency at 9 hpi, showing internalised myocardial debris (white arrowheads) in a
886 macrophage in a *Tg(myl7:GFP;mpeg1:mCherry)* larva. Scale bars = 50 μm for panels
887 a-f and 20 μm for panel (i). All images are 3D LSFM shown as maximum intensity
888 projections unless otherwise stated. *$p \leq 0.05$, **$p \leq 0.01$, ***$p \leq 0.001$ 2way ANOVA
889 followed by Holm-Sidak's Post-hoc tests.
890

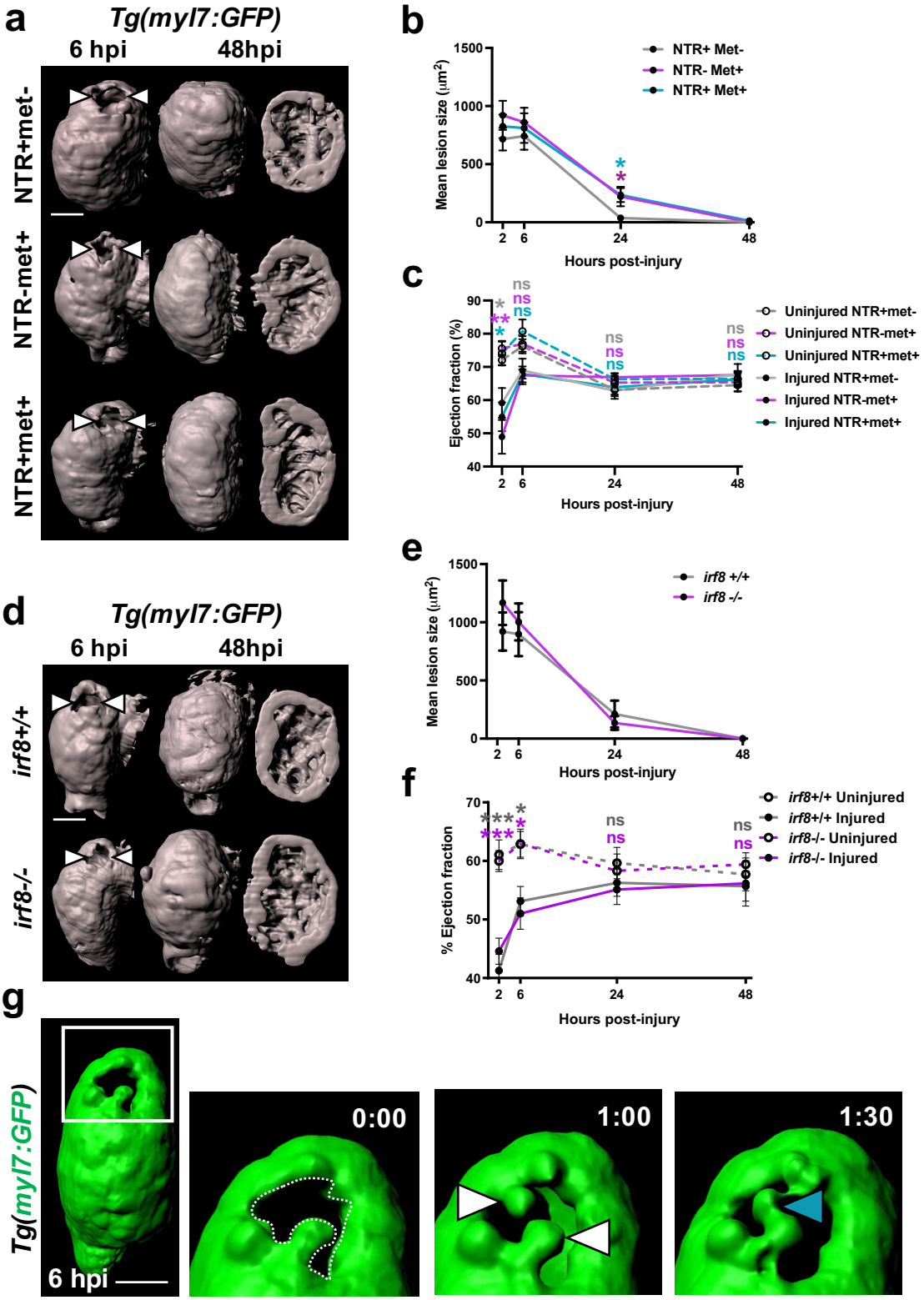

Figure 3: Macrophages not required for the recovery of cardiac structure or function.

(a) Representative GFP surface-renders of LSFM z-stacks of injured ventricles in *Tg(myl7:GFP;csfr1a:NfsB-mCherry)* larvae, macrophage ablation groups as indicated

896 in the figure. Abluminal myocardial surface is shown at 6 hpi (left) and abluminal and
897 luminal surfaces shown at 48 hpi following regeneration (middle & right). White
898 arrowheads = laser lesion. (b) Quantification of mean lesion size in injured
899 *Tg(myl7:GFP;csfr1a:NfsB-mCherry)* larvae per macrophage ablation group, n=11-22.
900 (c) Quantification of ventricular ejection fraction in uninjured and injured
901 *Tg(myl7:GFP;csfr1a:NfsB-mCherry)* larvae per macrophage ablation group, n=10-12.
902 (d) Representative GFP surface-renders of light-sheet-acquired z-stacks of injured
903 ventricles from *irf8*$^{+/+}$ and *irf8*$^{-/-}$ *Tg(myl7:GFP)* larvae. Abluminal myocardial surface is
904 shown at 6 hpi (left) and abluminal and luminal surfaces shown at 48 hpi following
905 regeneration (middle & right). White arrowheads = laser lesion. (e) Quantification of
906 mean lesion size in injured *irf8*$^{+/+}$ and *irf8*$^{-/-}$ *Tg(myl7:GFP)* larvae, n=15. (f)
907 Quantification of ventricular ejection fraction in uninjured and injured *irf8*$^{+/+}$ and *irf8*$^{-/-}$
908 *Tg(myl7:GFP)* larvae n=15-20. (g) Time-lapse timepoints of a GFP-surface-rendered,
909 injured *Tg(myl7:GFP)* ventricle from 6 hpi. White box = zoom panel; white arrowheads
910 = myocardial buds, cyan arrowhead = myocardial bridge. *$p \leq 0.05$, ***$p \leq 0.001$ 2way
911 ANOVA followed by Holm-Sidak's Post-hoc tests. Scale bars = 50 μm
912

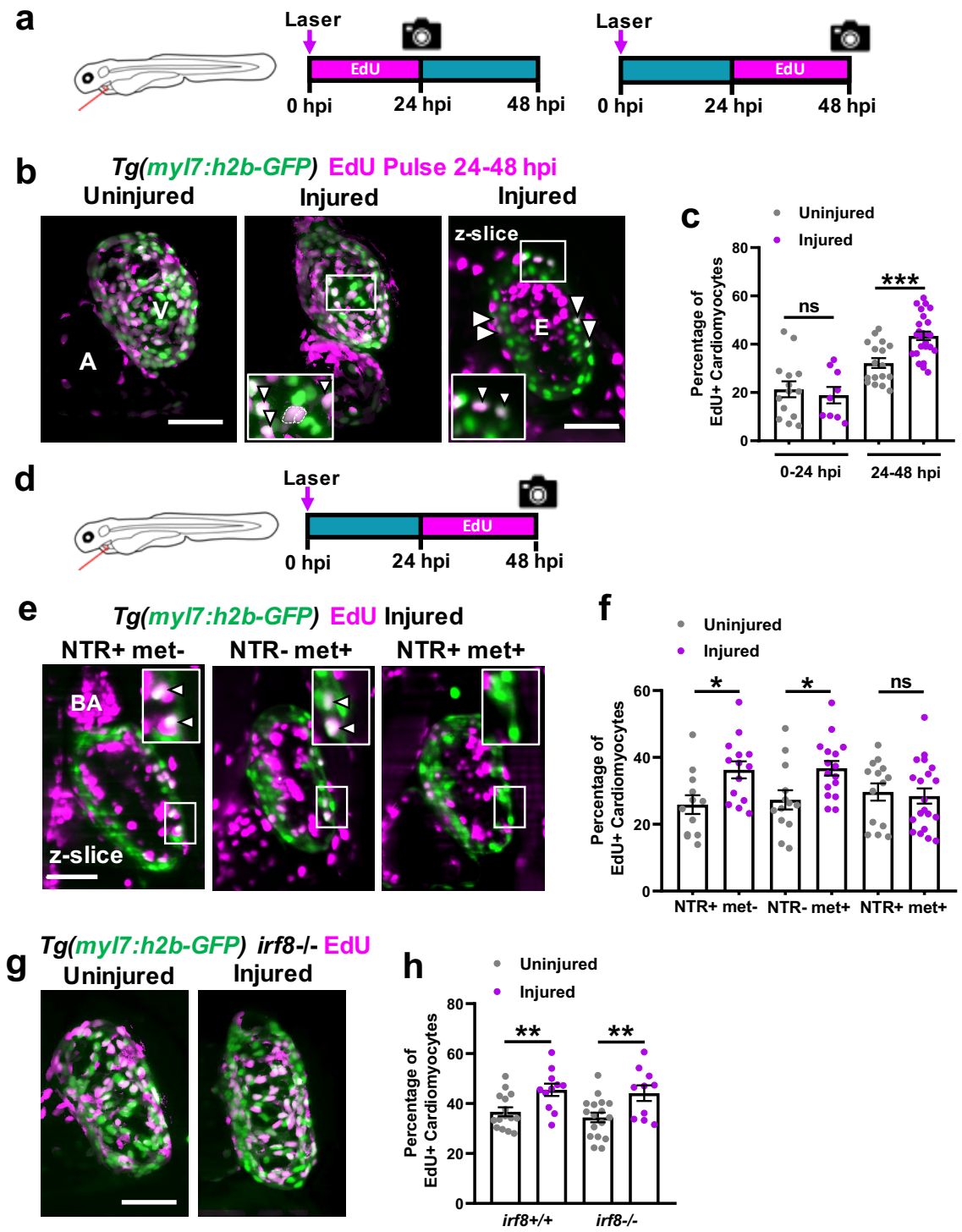

Figure 4: Macrophage ablation abolishes injury-dependent cardiomyocyte proliferation.

(a) Schematic illustrating EdU pulse strategy for labelling proliferating cardiomyocytes over 0-24 hpi (left) and 24-48 hpi (right). (b) Representative images of EdU-stained hearts from *Tg(myl7:h2b-GFP)* at 48 hpi. Non-myocardial EdU signal is excluded post-acquisition to allow interpretable maximal intensity projections (MIPs). A = atrium, v =

920 ventricle; white boxes = zoom panels; white arrowheads = EdU+ cardiomyocyte nuclei
921 and dashed line = outline of dividing cardiomyocyte daughter nuclei. (c) Quantification
922 of the percentage of ventricular EdU+ cardiomyocytes in uninjured and injured
923 *Tg(myl7:h2b-GFP)* hearts pulsed over 0-24 hpi or 24-48 hpi. ****p≤0.001* unpaired t
924 test. (d) Schematic illustrating EdU pulse strategy for labelling proliferating
925 cardiomyocytes over 24-48 hpi in *Tg(myl7:h2b-GFP;csfr1a:NfsB-mCherry)* larvae per
926 standard macrophage ablation groups. (e) Representative images of EdU-stained
927 hearts from *Tg(myl7:h2b-GFP;csfr1a:NfsB-mCherry)* acquired by light-sheet
928 microscopy at 48 hpi. White boxes = zoom panels; white arrowheads = EdU+
929 cardiomyocyte nuclei and BA = bulbous arteriosus. (f) Quantification of the percentage
930 of ventricular EdU+ cardiomyocytes in uninjured and injured *Tg(myl7:h2b-*
931 *GFP;csfr1a:NfsB-mCherry)* hearts pulsed over 24-48 hpi. **p≤0.05* Kruskal-Wallis test
932 and Dunn's multiple comparison post-hoc test. (g) Representative images of uninjured
933 and injured EdU-stained hearts from *irf8*$^{-/-}$ *Tg(myl7:h2b-GFP)* acquired by light-sheet
934 microscopy at 48 hpi. Non-myocardial EdU signal is excluded post-acquisition to allow
935 interpretable maximal intensity projections. (h) Quantification of the percentage of
936 ventricular EdU+ cardiomyocytes in uninjured and injured *irf8*$^{+/+}$ and *irf8*$^{-/-}$
937 *Tg(myl7:h2b-GFP)* hearts pulsed 24-48 hpi. All images are maximum intensity
938 projections of 3D LSFM stacks, unless otherwise stated. Scale bars = 50 μm. ***p≤0.01*
939 unpaired t test
940

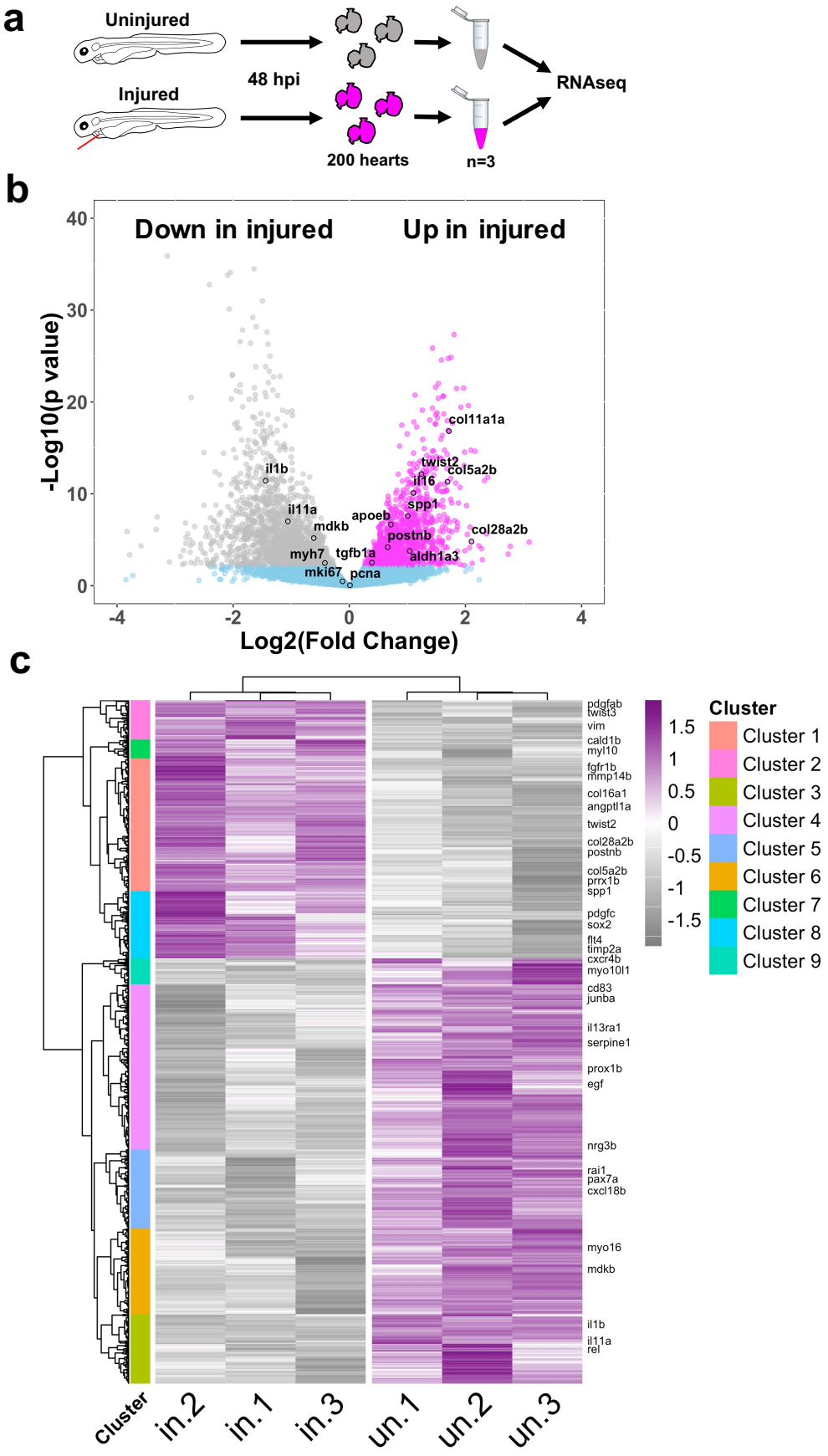

Figure 5: Bulk RNAseq analysis of larval hearts following injury

943 (a) Schematic illustrating the extraction of uninjured and injured hearts at 48 hpi and
944 the pooling of 200 hearts per biological replicate for RNAseq, n=3. (b) Volcano plot
945 showing the Log_2(Fold Change) and $-Log_{10}$(p value) for transcripts of each detected
946 gene. Genes whose adjusted p values fall below 0.05 are deemed statistically non-
947 significant and coloured blue. Genes up regulated in injured hearts are coloured
948 magenta and those upregulated in uninjured hearts are coloured grey. (c) Heatmap
949 displaying statistically significantly differentially expressed genes with a Log_2(Fold
950 Change) >0.5. Genes were hierarchically clustered by Pearson correlation with z
951 scaling. Clusters are indicated on the left with their dendrogram. Magenta = high
952 expression; grey = low expression. Genes with relevance to cardiac regeneration are
953 highlighted as annotations on the right of the plot. n=3
954

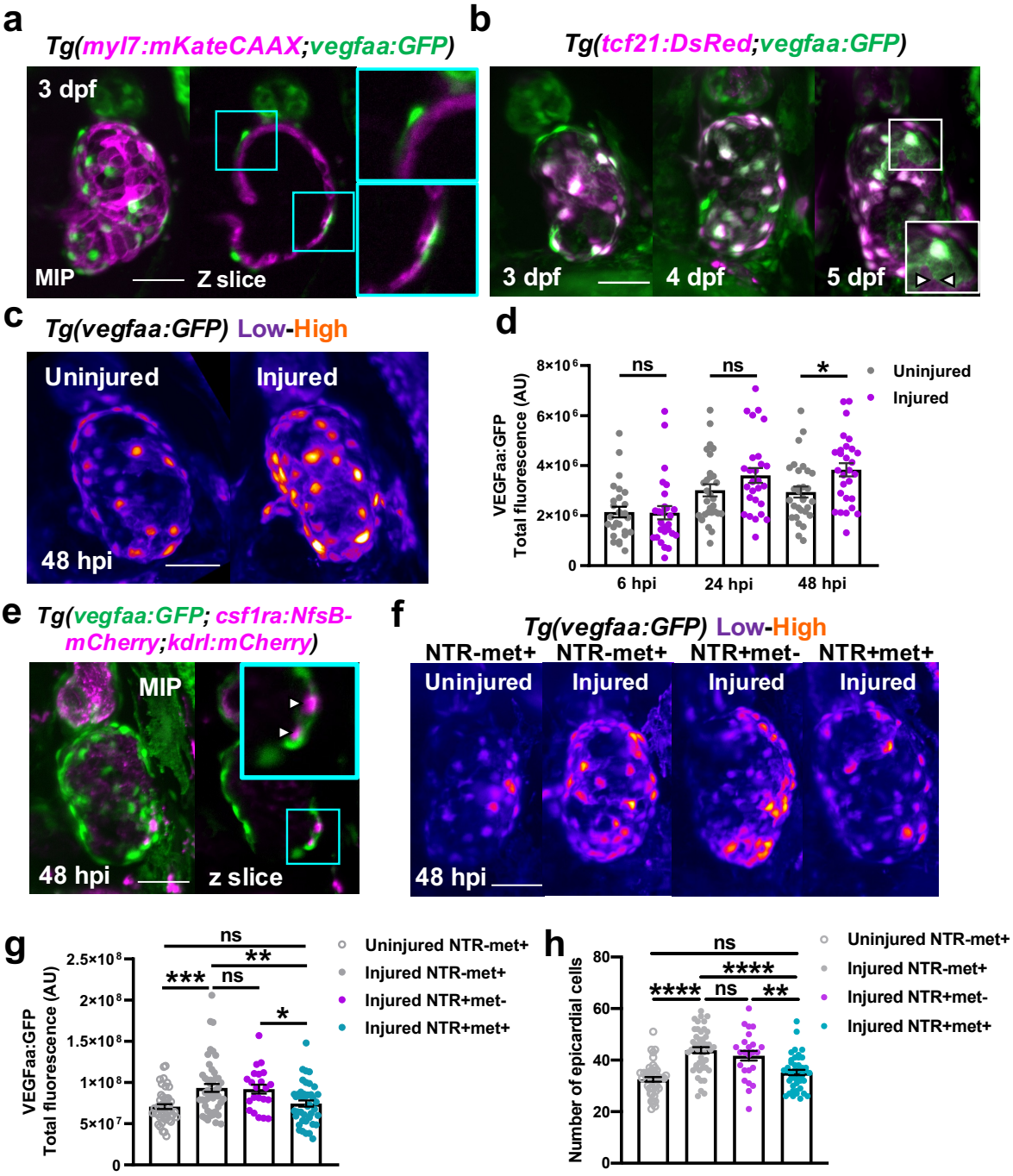

Figure 6: Macrophages stimulate epicardial cell number expansion following cardiac injury.

(a) Representative LSFM image of an uninjured 3 dpf ventricle from a *Tg(myl7:mKateCAAX;myl7:h2b-GFP)* larva showing vegfaa+ cells (green) overlying myocardium (magenta). Cyan box = zoom panel. (b) Representative images of 3, 4 and 5 dpf ventricles from a *Tg(tcf21:DsRed;vegfaa:GFP)* larvae acquired by LSFM, showing high colocalization of vegfaa with epicardial marker tcf21. White arrowheads = heterogenous marker expression and white box = zoom panel. (c) Representative

964 images of uninjured and injured ventricles from *Tg(vegfaa:GFP)* larvae acquired at 48
965 hpi by LSFM. “Heat” LUT applied to highlight increased intensity of epicardial
966 vegfaa:GFP in injured hearts. (d) Quantification of total ventricular VEGFaa:GFP
967 fluorescence in uninjured and injured hearts over standard injury model timepoints,
968 n=28-30. *$p \leq 0.05$ One way ANOVA followed by Holms-Sidak’s multiple comparison
969 Post-hoc tests. (e) Representative image of a ventricle from a
970 *Tg(vegfaa:GFP;csfr1a:NfsB-mCherry;kdrl:hsa.HRAS-mCherry)* (abbreviated to
971 kdrl:mCherry) larva at 48 hpi showing macrophages in the epicardial-myocardial niche
972 (white arrowheads). Cyan box = zoom panel. (f) Representative LSFM images of
973 uninjured and injured ventricles from *Tg(vegfaa:GFP;csfr1a:NfsB-mCherry)* larvae
974 from metronidazole-nitroreductase macrophage ablation groups at 48 hpi. “Heat” LUT
975 is applied to highlight increase in overall fluorescence in injured groups except
976 NTR+met+. (g) Quantification of total vegfaa:GFP fluorescence (g) and epicardial cell
977 number (h) in uninjured and injured ventricles from *Tg(vegfaa:GFP;csfr1a:NfsB-*
978 *mCherry)* larvae from metronidazole-nitroreductase macrophage ablation groups at
979 48 hpi. All images are maximum intensity projections of 3D LSFM stacks. Scale bars
980 = 50 μm, n=46. *$p \leq 0.05$, **$p \leq 0.01$, ***$p \leq 0.001$ One way ANOVA followed by Holms-
981 Sidak’s multiple comparison Post-hoc tests.
982
983

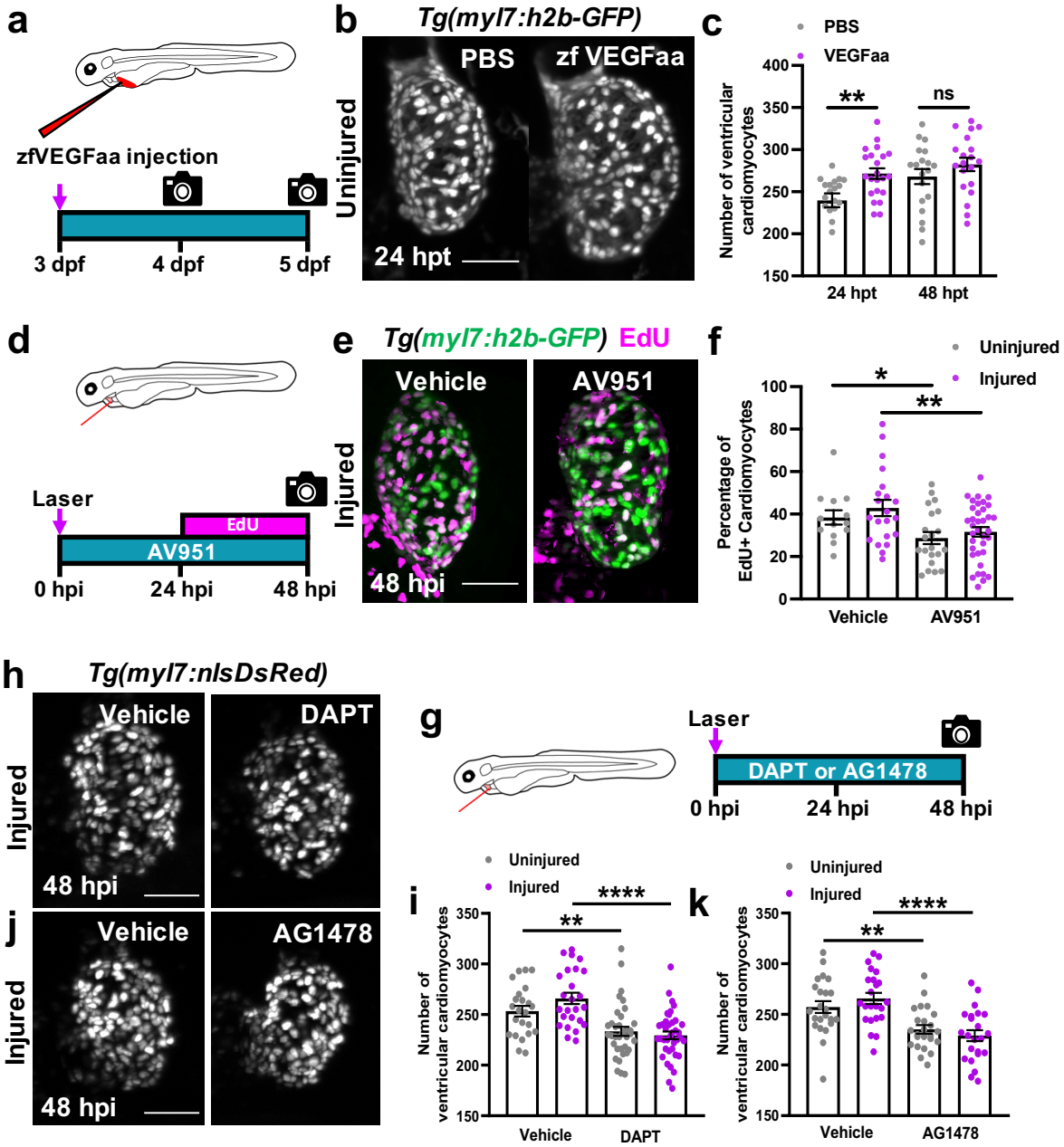

Figure 7: VEGFaa signalling is both sufficient and necessary to drive cardiomyocyte proliferation.

(a) Schematic illustrating zfVEGFaa treatment strategy via microinjection into the common cardinal vein of uninjured larvae at 72 hpi. (b) Representative LSFM images of *Tg(myl7:h2b-GFP)* larvae at 24 hpi treated with PBS 0.1% BSA or zfVEGFaa 0.1% BSA injection. (c) Quantification of ventricular cardiomyocyte number in *Tg(myl7:h2b-GFP)* larvae at 24 and 48 hpi treated with PBS 0.1% BSA or zfVEGFaa 0.1% BSA injection, n=20. ***p≤0.01* unpaired t test. (d) Schematic illustrating AV951 treatment and EdU pulsing strategy for uninjured and injured larvae. (e) Representative images of injured ventricles from *Tg(myl7:h2b-GFP)* larvae, EdU stained and bathed in vehicle

995 or AV951, imaged at 48 hpi by LSFM. Non-myocardial EdU signal is excluded post-
996 acquisition to allow interpretable maximal intensity projections (MIPs). (f)
997 Quantification of the percentage of EdU+ cardiomyocyte nuclei from uninjured and
998 injured ventricles from *Tg(myl7:h2b-GFP)* larvae, EdU stained and bathed in vehicle
999 or AV951, n=13-36. *$p \leq 0.05$, **$p \leq 0.01$ unpaired t test. (g) Schematic illustrating the
1000 treatment strategy for DAPT and AV951 bathing of uninjured and injured larvae. (h)
1001 Representative images of injured *Tg(myl7:nlsDsRed)* larvae treated with vehicle or
1002 DAPT, acquired at 48 hpi by LSFM. (i) Quantification of ventricular cardiomyocyte
1003 number in uninjured and injured *Tg(myl7:h2b-GFP)* larvae at 48 hpi treated with
1004 vehicle or DAPT, n=24-40. **$p \leq 0.01$, ****$p \leq 0.0001$ Unpaired t test.(j) Representative
1005 images of injured *Tg(myl7:nlsDsRed)* larvae treated with vehicle or AG1478, acquired
1006 at 48 hpi by LSFM. (k) Quantification of ventricular cardiomyocyte number in uninjured
1007 and injured *Tg(myl7:h2b-GFP)* larvae at 48 hpi treated with vehicle or AG1478, n=24.
1008 All images are maximum intensity projections of 3D LSFM stacks. **$p \leq 0.01$,
1009 ****$p \leq 0.0001$ Unpaired t test. Scale bars = 50 μm.

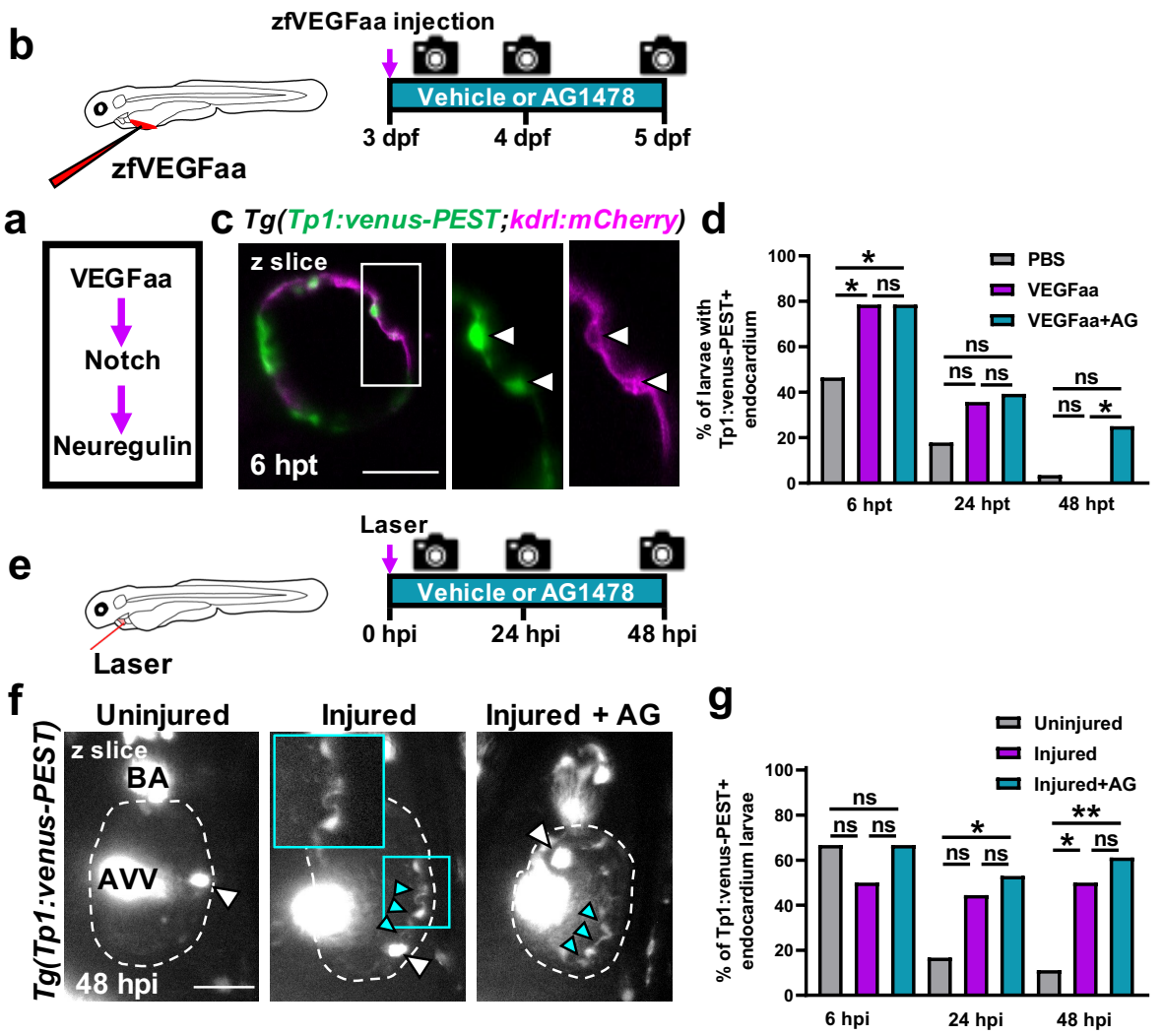

Figure 8: VEGFaa drives cardiomyocyte proliferation by endocardial notch signalling.

(a) Hypothesised signalling pathway active in uninjured and injured larval hearts driving cardiomyocyte proliferation. (b) Schematic illustrating the treatment strategy for the injection of uninjured larvae with zfVEGFaa and continuous bathing in AG1478 solution. (c) Representative LSFM-acquired z plane showing notch expression colocalising with endocardium in *Tg(Tp1:venus-PEST;kdrl:hsa.HRAS-mCherry),* abbreviated in the figure to *Tg(Tp1:venus-PEST;kdrl:mCherry).* AG1478 abbreviated to AG, white box = zoom panel. (d) Quantification of the proportion of larvae with notch+ endocardium at 6, 24, and 48 hpt following zfVEGFaa injection and bathing in AG1478, n=28. *$p \leq 0.05$ Fisher's exact test. (e) Schematic illustrating the treatment strategy for the lasering of larvae and continuous bathing in AG1478 solution. (f) Representative z plane images of uninjured, injured and injured AG-treated ventricles from *Tg(tp1:venus-PEST)* larvae acquired by light-sheet microscopy at 48 hpi. BA =

1025 bulbous arteriosus; AVV = atrioventricular valve; white arrowheads =laterally inhibited
1026 cardiomyocytes, cyan arrowheads = notch+ endocardium; cyan box = zoom panel. (g)
1027 Quantification of the proportion of larvae with notch+ endocardium at 6, 24, and 48 hpt
1028 following laser injury and bathing in AG1478, n=18. All images are maximum intensity
1029 projections of 3D LSFM stacks unless otherwise stated. *$p \leq 0.05$, **$p \leq 0.01$ Fisher's
1030 exact test. Scale bars = 50 μm.
1031
1032 **Supplementary figures**
1033

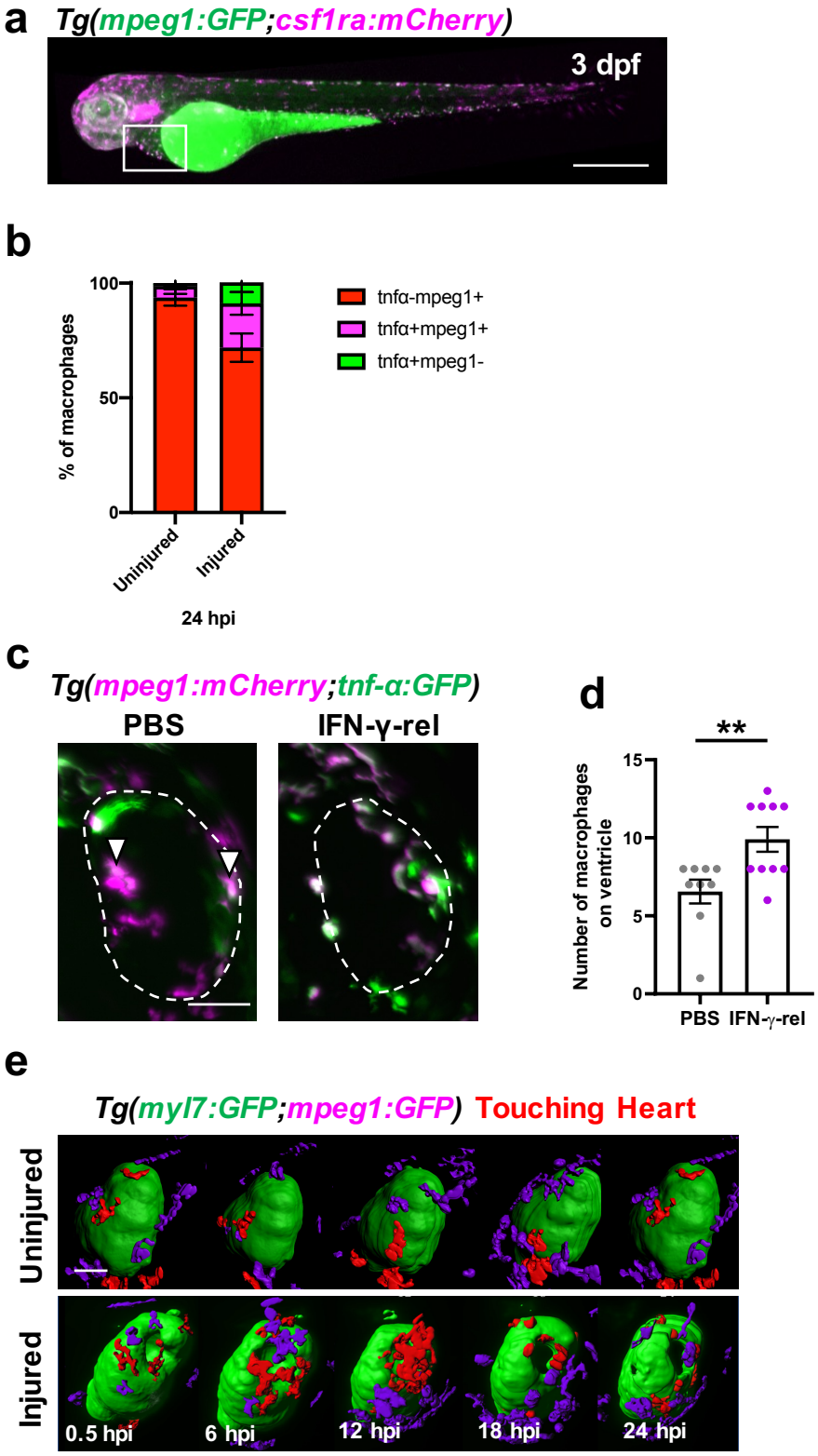

1034

1035 **Supplementary figure 1: Cardiac macrophage phenotype in larval zebrafish is**
1036 **plastic and can be polarised to tnfa+ by IFN-γ-rel.**
1037 (a) Representative epifluorescence image of a 3 dpf *Tg(mpeg1:GFP;csf1ra:NfsB-*
1038 *mCherry)* abbreviated to *Tg(mpeg1:GFP;csf1ra:mCherry)* in the figure, showing an

1039 anterior-posterior polarity in macrophage expression of csf1ra (higher proportion of
1040 anterior macrophages were csf1ra+). White box = indicated pericardial area. Scale bar
1041 = 500μm. (b) Quantification of the proportion of macrophages that are tnfa-mpeg1+,
1042 tnfa+mpeg1+ and tnfa+mpeg1- on hearts in uninjured and injured larvae at 24 hpi. (c)
1043 Representative images of hearts from *Tg(mpeg1:mCherry;tnfa:GFP)* larvae at 24 hpi
1044 injected with PBS or IFN-γ-rel. White dashed line = outline of the ventricle; and white
1045 arrowheads = tnfa+mpeg1+ macrophages. Scale bar = 50μm. (d) Quantification of the
1046 number of macrophages on the injured ventricle at 24 hpi after injection at 0 hpi with
1047 PBS or IFN-γ-rel. (e) Time-lapse timepoints of *Tg(myl7:GFP;mpeg1:mCherry)* hearts
1048 acquired by heartbeat-synchronised LSFM, surface rendered and colour-coded to
1049 show myocardium in green, macrophages on the heart in red and macrophages
1050 elsewhere in purple. Macrophages can be seen to change from stellate to rounded
1051 over time following injury. Scale bar = 50μm.
1052

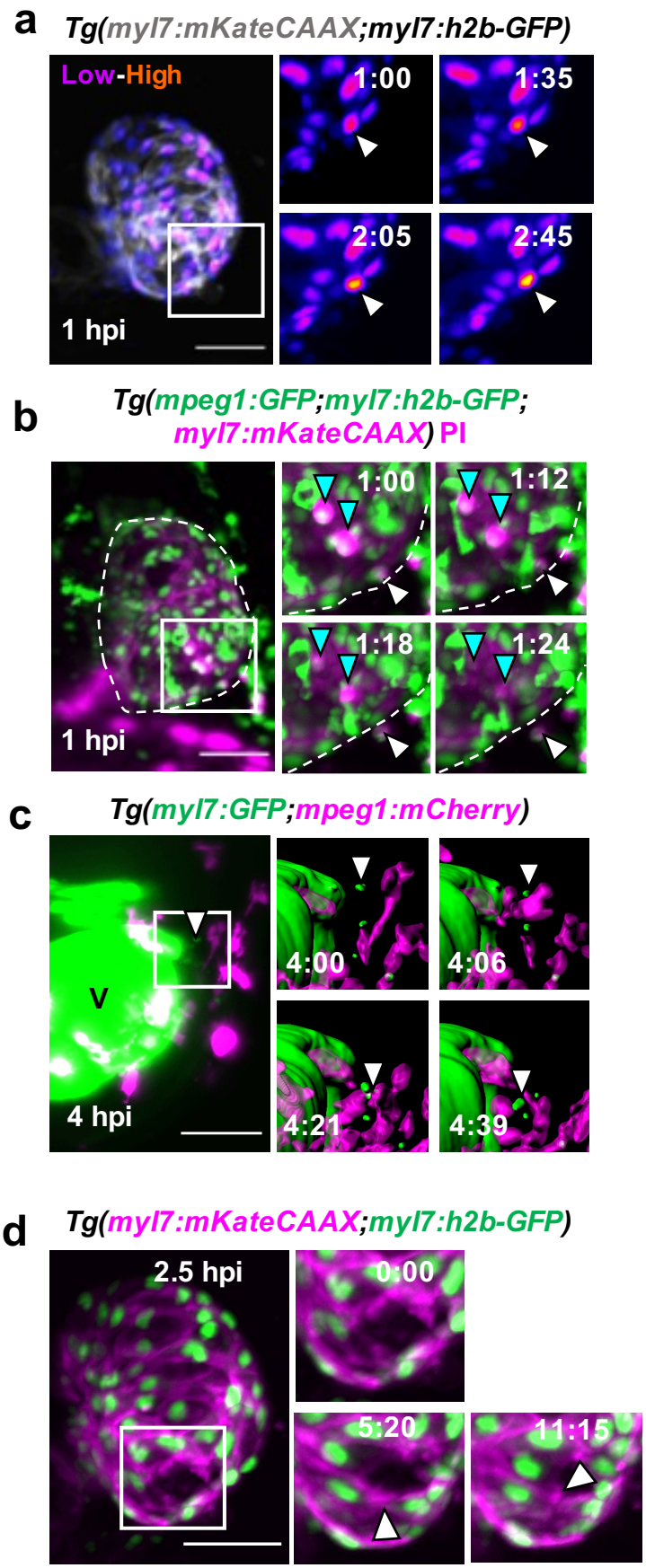
a
Tg(myl7:mKateCAAX;myl7:h2b-GFP)
Low-High
1:00
1:35
2:05
2:45
1 hpi
b
Tg(mpeg1:GFP;myl7:h2b-GFP;
myl7:mKateCAAX) PI
1:00
1:12
1:18
1:24
1 hpi
c
Tg(myl7:GFP;mpeg1:mCherry)
V
4:00
4:06
4:21
4:39
4 hpi
d
Tg(myl7:mKateCAAX;myl7:h2b-GFP)
2.5 hpi
0:00
5:20
11:15

1053

1054 **Supplementary figure 2: Heartbeat-synchronised lightsheet-acquired time-lapse**
1055 **stills**
1056 (a) Time-lapse stills of injured *Tg(myl7:h2b-GFP;myl7:mKateCAAX)* ventricles
1057 imaged from 1 hpi. GFP intensity show by heat LUT, white arrowhead = apoptotic
1058 cardiomyocyte/condensing nucleus, white box = zoom panel. (b) Time-lapse stills of
1059 injured *Tg(myl7:h2b-GFP;myl7:mKateCAAX;mpeg1:GFP)* ventricles imaged from 1
1060 hpi by heart-synchronised light-sheet imaging. Round GFP^{low} = cardiomyocyte nuclei
1061 and stellate GFP^{high} =macrophages. Cyan arrowheads = Necrotic cardiomyocyte
1062 nuclei and white arrowheads = expelled necrotic cardiomyocyte, white box = zoom
1063 panel. (c) Time-lapse stills of an injured *Tg(myl7:GFP;mpeg1:mCherry)* ventricle from
1064 4 hpi where the full size panel has high gain in the GFP channel to highlight GFP^{low}
1065 myocardial debris and zoom panels (area indicated by white box) are surface rendered
1066 to highlight removal of myocardium (green) by macrophages (magenta). V = high gain
1067 ventricle, white arrowhead = myocardial debris. (d) Time-lapse stills of an injured
1068 *Tg(myl7:mKateCAAX;myl7:h2b-GFP)* ventricle from 2.5 hpi. White box = zoom panel,
1069 white arrowheads = cell-cell junctions
1070

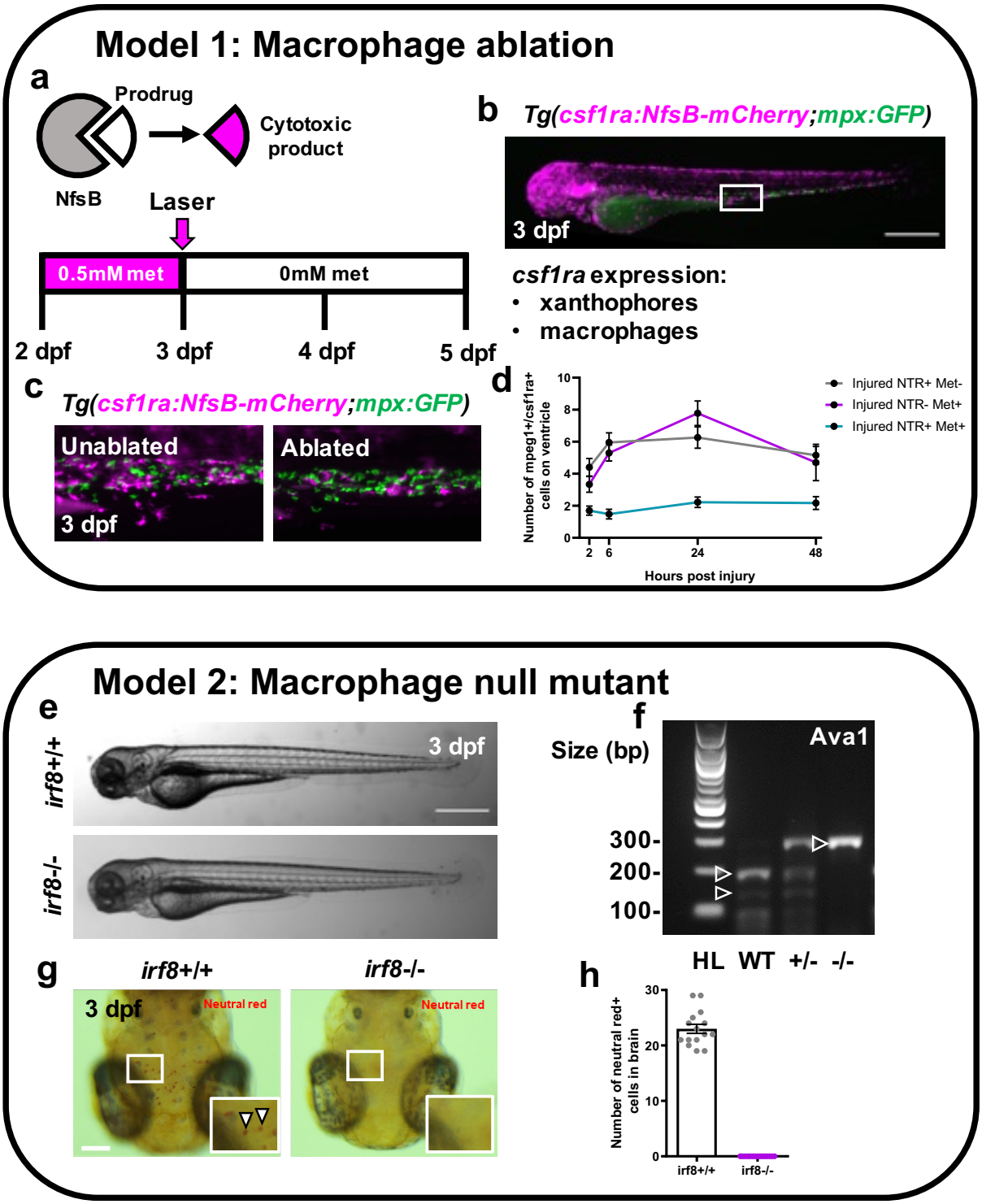

Supplementary figure 3: Macrophages can be pharmacologically ablated or developmentally blocked genetically.

(a) Schematic illustrating how nitroreductase enzyme 'NfsB' catabolises prodrug 'metronidazole' to form a cytotoxic biproduct. (b) Representative epifluorescence image of a *Tg(csf1ra:NfsB-mCherry;mpx:GFP*) 3 dpf larva (abbreviated to *Tg(csf1ra:mCherry;mpx:GFP)* in all panels), white box = caudal haematopoietic tissue,

magenta = macrophages and green = neutrophils (CHT) (c) Representative images of ablated and unablated macrophages in the CHT, size and location indicated in (b)) in *Tg(csf1ra:mCherry;mpx:GFP)* 3dpf larvae. Macrophages are ablated and only apoptotic bodies remain but not neutrophils are unaffected. (d) Quantification of macrophages at standard timepoints, marked by either mpeg1 or csfr1a on the injured ventricle in each of the NTR=metronidazole ablation model's treatment groups NTR+Met-, NTR-Met+ and NTR+Met+. Macrophage ablation can be seen to abolish the macrophage response (e) Representative brightfield images of *irf8*$^{+/+}$ and *irf8*$^{-/-}$ larvae at 3 dpf. (f) Representative 1% agarose gel displaying Ava1 restriction digest band pattern for WT, *irf8* heterozygous and homozygous mutants. (g) Representative dorsal view brightfield image of 3 dpf larval heads stained with neutral red vital dye with white zoom panel highlighting stained macrophages (microglia) (red) in *irf8+/+* but not *irf8*$^{-/-}$ larvae. (h) Quantification of the number of neutral red positive stained cells (macrophages/microglia) in larval brains of *irf8*$^{+/+}$ and *irf8*$^{-/-}$ at 3 dpf showing *irf8*$^{-/-}$ larvae to be macrophage-null. Scale bar = 500μm (b & e), 100μm (g).

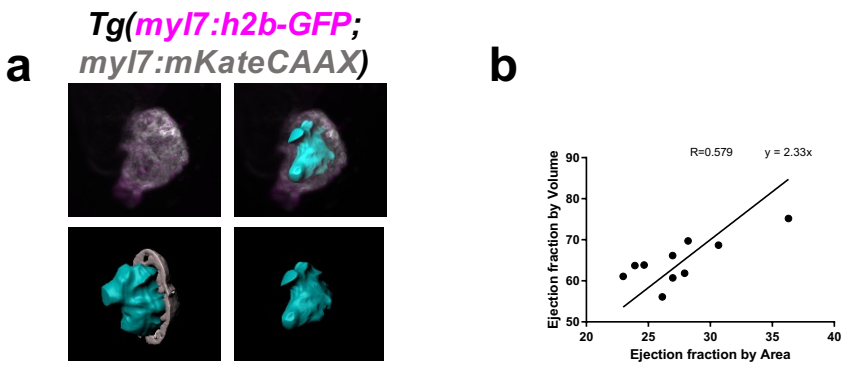

Supplementary figure 4: Ejection fraction by area is proportional to ejection fraction by volume.

(a) Representative IMARIS-generated image showing a rendered ventricular myocardium (grey render), rendered chamber volume (cyan) and MIP of 3D heartbeat-synchronised LSFM scan of a 3 dpf heart (ventricle) in diastole. Image acquired from a *Tg(myl7:h2b-GFP;myl7:mKateCAAX)* larva. (b) Quantification of ejection fraction by area (calculated from diastolic and systolic lateral brightfield images) and by volume

1105 (calculated from surface renders of luminal volumes in diastole and systole) for n=10
1106 fish.
1107

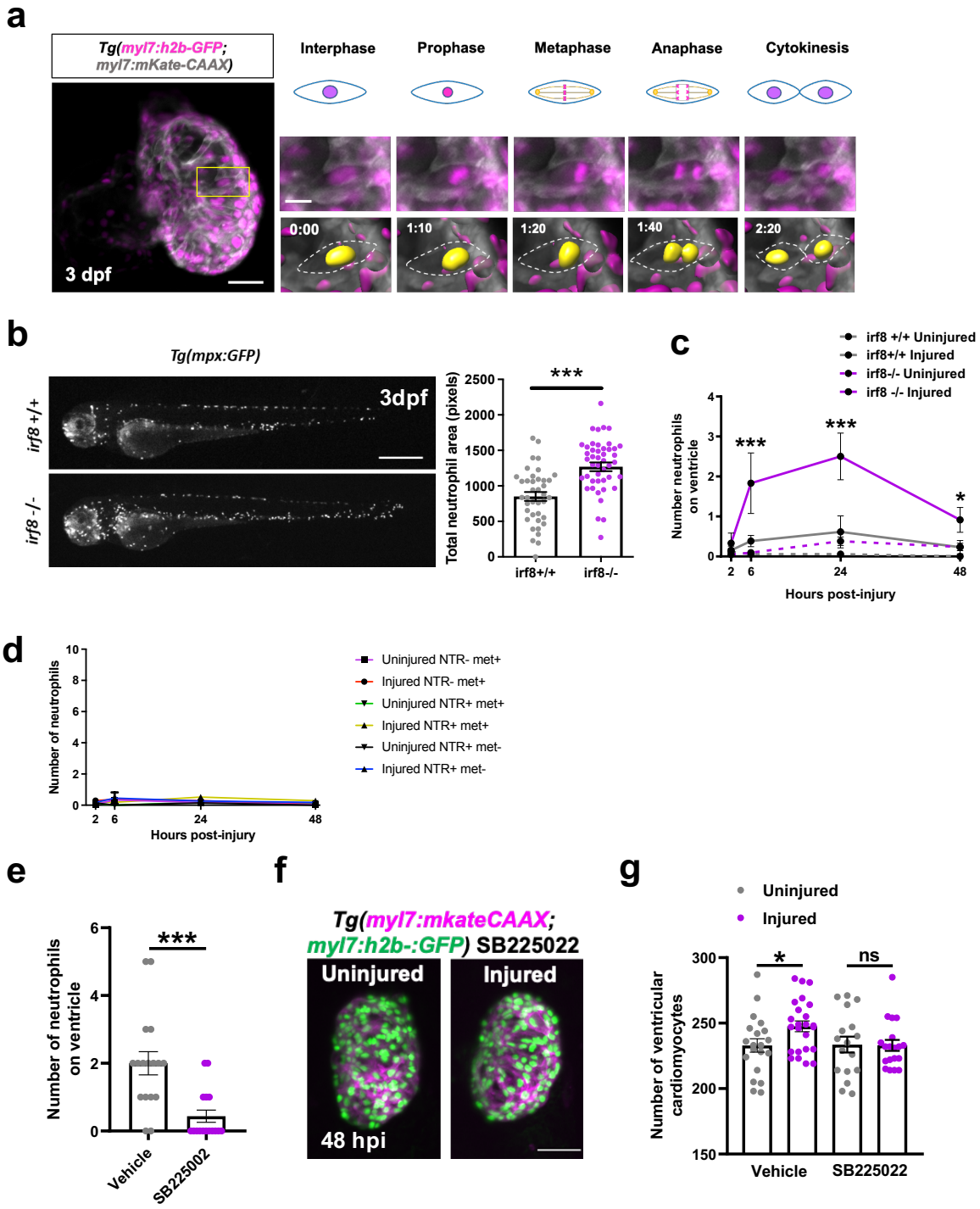

1108

1109 **Supplementary figure 5: *irf8*$^{-/-}$ larvae have a larger neutrophil response to**
1110 **cardiac injury than *irf8*$^{+/+}$.**

1111 (a) Representative timepoint images from heartbeat-synchronised LSFM time-lapse
1112 of a laser-injured 3 dpf *Tg(myl7:h2b-GFP;myl7:mKateCAAX)* larva showing an

1113 example of each phase of complete cell division of a single cardiomyocyte, typical of
1114 larval hearts. Yellow box = zoom panel; left scale bar = 30 μm; right scale bar = 10
1115 μm. Timestamps post-injury indicated in figure. (b) Representative whole larva
1116 epifluorescence image of *irf8*$^{-/-}$ and *irf8*$^{+/+}$ *Tg(mpx:GFP)* larvae showing *irf8*$^{-/-}$ to have
1117 greater global neutrophil numbers (scale bar = 500 μm), quantified in the graph (right).
1118 ***$p \leq 0.001$. t test, n=39-46. (c) Quantification of neutrophil numbers at the ventricle in
1119 uninjured and injured *irf8*$^{+/+}$ and *irf8*$^{-/-}$ larvae at the standard laser-injury model
1120 timepoints, showing *irf8*$^{-/-}$ larvae to have a significantly greater neutrophil response.
1121 n=17-25. (d) Quantification of neutrophil numbers at the ventricle in uninjured and
1122 injured NTR-met+, NTR+met+ and NTR+met- larvae at the standard laser-injury
1123 model timepoints. All metronidazole-nitroreductase treatment groups to have a
1124 minimal neutrophil response and therefore no neutrophil compensation in the
1125 macrophage ablated group NTR+met+, n=17-24. (e) Quantification of the number of
1126 recruited neutrophils at the injured ventricle in at 24 hpi in *Tg(myl7:h2b-*
1127 *GFP;myl7:mKateCAAX)* larvae bathed in vehicle or SB225002 from -2 to +24 hpi
1128 showing SB225002 to significantly reduce neutrophil number, n=17. (f) Representative
1129 light-sheet acquired images of uninjured and injured *irf8*$^{-/-}$ *Tg(myl7:h2b-*
1130 *GFP;myl7:mKateCAAX)* ventricles at 48 hpi following treatment with SB225002 from
1131 -2 to +24 hpi, scale bar = 50 μm. (g) Quantification of ventricular cardiomyocyte
1132 number in uninjured and injured *irf8*$^{-/-}$ *Tg(myl7:h2b-GFP;myl7:mKateCAAX)* ventricles
1133 at 48 hpi following treatment with vehicle or SB225002 -2 to 24 hpi, n=17-20, *$p \leq 0.05$
1134 t test
1135

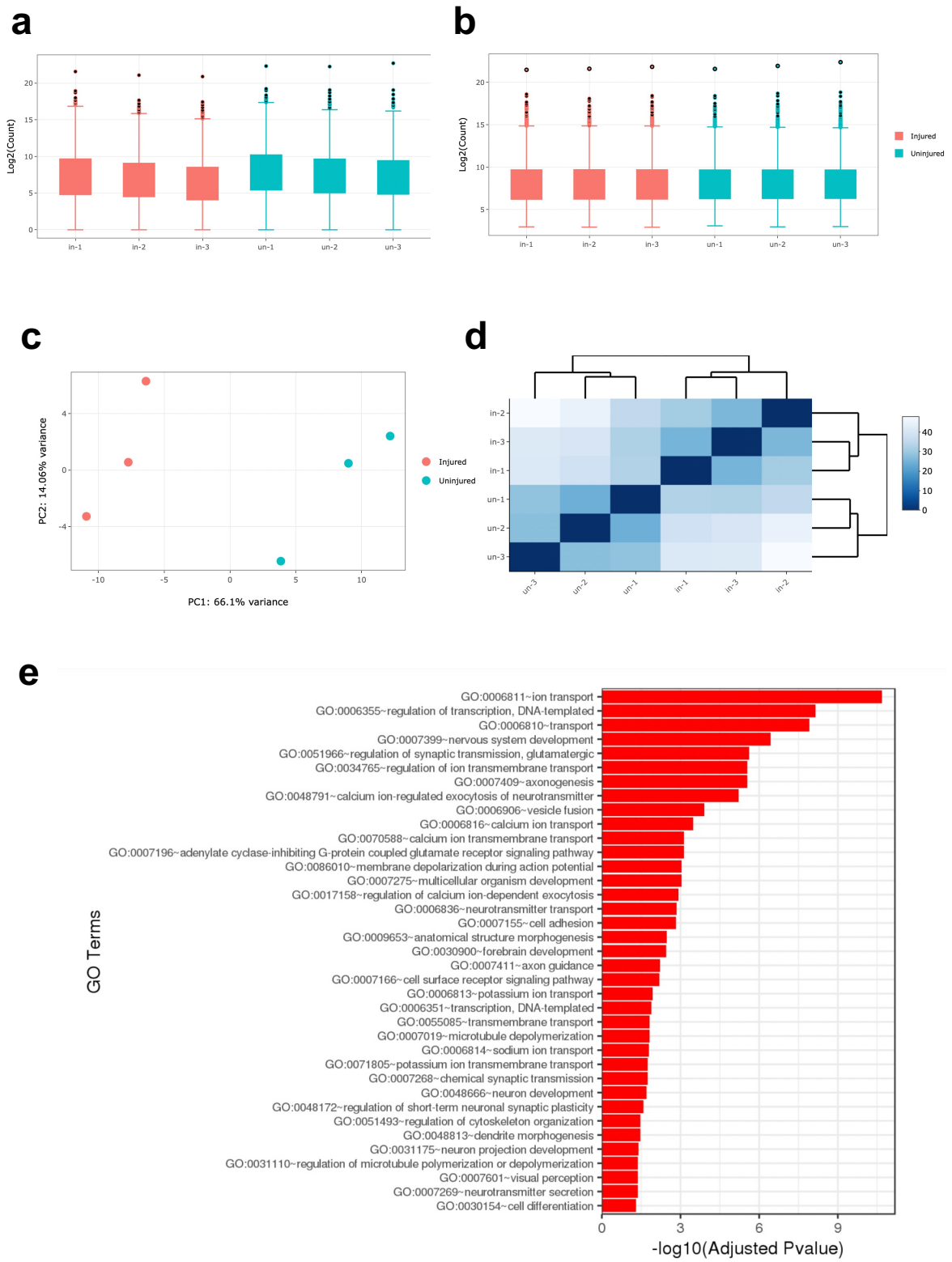

Supplementary figure 6: Bulk RNAseq analysis of uninjured and injured larval hearts

(a) Box plot illustrating the distribution of reads before (a) and after normalisation (b) Principal component analysis of samples, illustrating relative intragroup sample

similarity. (c) Distance matrix illustrating pairwise sample similarity. (e) Plot showing gene ontology terms that were significantly enriched by Fishers exact test for significantly (padj<0.05) differentially expressed genes between uninjured and injured hearts at 48 hpi.

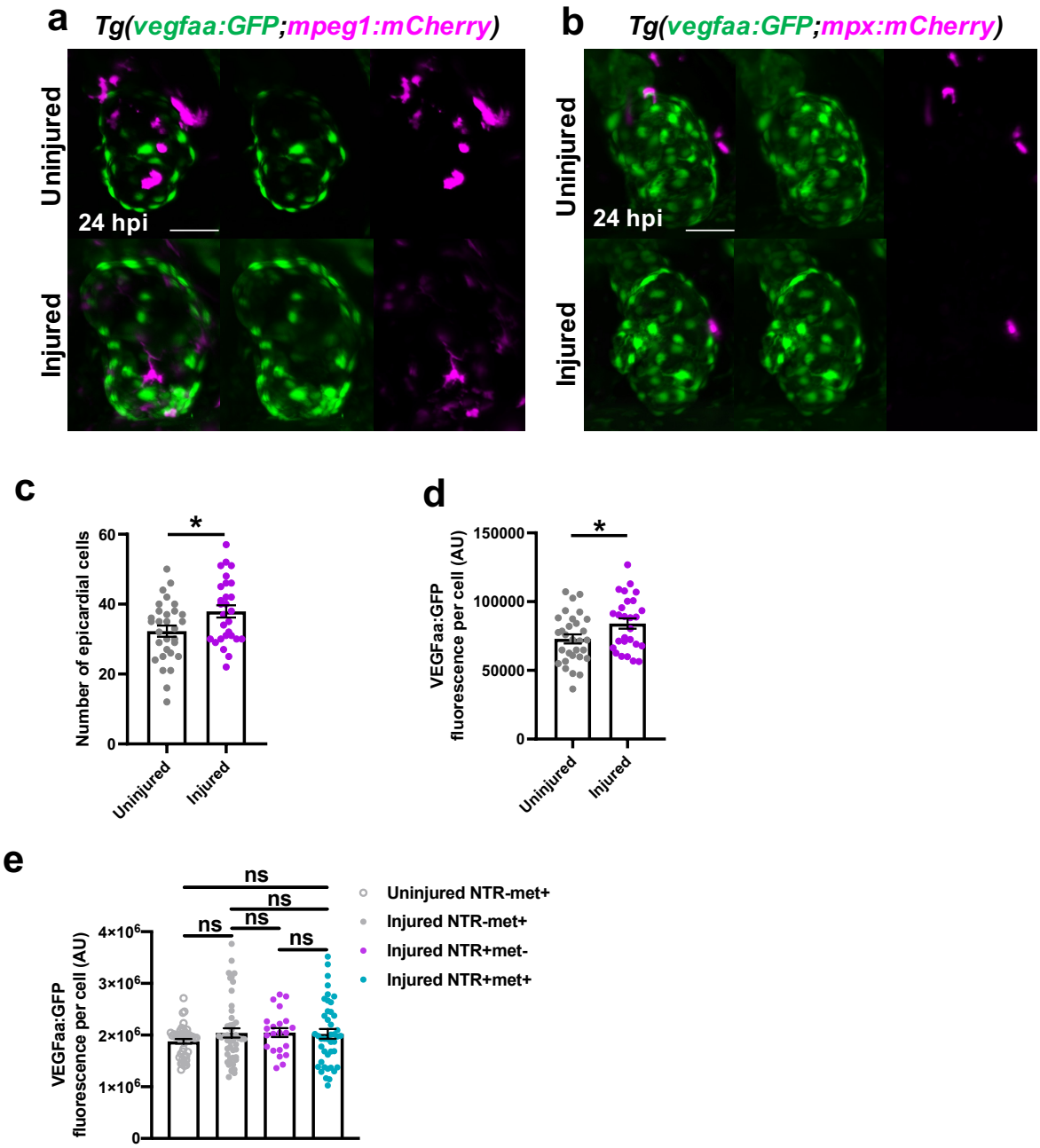

Supplementary figure 7: *vegfaa:GFP* expression does not colocalize with macrophages or neutrophils following larval heart injury.

(a) Representative LSFM image of an injured *Tg(vegfaa:GFP;mpeg1:mCherry)* heart 24 hpi showing *vegfaa:GFP* expression only in the epicardium and not in

1151 macrophages, scale bar = 100μm. (b) Representative LSFM image of an injured
1152 *Tg(vegfaa:GFP;mpx:mCherry)* heart 24 hpi showing VEGFaa expression only in the
1153 epicardium and not in neutrophils, scale bar = 100μm. (c) Quantification of the number
1154 of epicardial cells, as marked by vegfaa:GFP, on injured ventricles at 48 hpi in
1155 uninjured and injured larvae, n=30. *$p \leq 0.05$ t test (d) Quantification of the average
1156 vegfaa:GFP expression of epicardial cells per cell, on injured ventricles at 48 hpi in
1157 uninjured and injured larvae, n=30. *$p \leq 0.05$ t test (e) Quantification of average
1158 vegfaa:GFP fluorescence per cell in metronidazole-nitroreductase ablation model
1159 groups at 48 hpi, n=22-44. One-way ANOVA followed by Holm-Sidak's multiple
1160 comparisons Post-hoc test.
1161
1162
1163 **References**
1164

1165 1. Ohnmacht, J., Yang, Y., Maurer, G. W., Barreiro-Iglesias, A., Tsarouchas, T.
1166 M., Wehner, D., Sieger, D., Becker, C. G. & Becker, T. Spinal motor neurons
1167 are regenerated after mechanical lesion and genetic ablation in larval
1168 zebrafish. *Dev.* **143**, 1464–1474 (2016).
1169 2. Becker, C. G., Lieberoth, B. C., Morellini, F., Feldner, J., Becker, T. &
1170 Schachner, M. L1.1 is involved in spinal cord regeneration in adult zebrafish. *J.*
1171 *Neurosci.* **24**, 7837–7842 (2004).
1172 3. Bensimon-Brito, A., Ramkumar, S., Boezio, G. L. M., Guenther, S., Kuenne,
1173 C., Helker, C. S. M., Sánchez-Iranzo, H., Iloska, D., Piesker, J., Pullamsetti, S.,
1174 Mercader, N., Beis, D. & Stainier, D. Y. R. TGF-β Signaling Promotes Tissue
1175 Formation during Cardiac Valve Regeneration in Adult Zebrafish. *Dev. Cell* **0**,
1176 (2019).
1177 4. Sander, V., Davidson, A. J., Sander, V. & Davidson, A. J. Kidney Injury and
1178 Regeneration in Zebrafish. *Semin. Nephrol.* **34**, 437–444 (2014).
1179 5. Basu Mallik, S., Jayashree, B. S. & Shenoy, R. R. Epigenetic modulation of
1180 macrophage polarization- perspectives in diabetic wounds. *J. Diabetes*
1181 *Complications* **0**, (2018).
1182 6. González-Rosa, J. M., Martín, V., Peralta, M., Torres, M. & Mercader, N.
1183 Extensive scar formation and regression during heart regeneration after
1184 cryoinjury in zebrafish. *Development* **138**, 1663–1674 (2011).

1185 7. Leuschner, F., Rauch, P. J., Ueno, T., Gorbatov, R., Marinelli, B., Lee, W. W.,
1186 Dutta, P., Wei, Y., Robbins, C., Iwamoto, Y., Sena, B., Chudnovskiy, A.,
1187 Panizzi, P., Keliher, E., Higgins, J. M., Libby, P., Moskowitz, M. A., Pittet, M. J.,
1188 Swirski, F. K., Weissleder, R. & Nahrendorf, M. Rapid monocyte kinetics in
1189 acute myocardial infarction are sustained by extramedullary monocytopoiesis.
1190 *J. Exp. Med.* **209**, 123–37 (2012).
1191 8. Murry, C. E., Reinecke, H. & Pabon, L. M. Regeneration Gaps. Observations
1192 on Stem Cells and Cardiac Repair. *Journal of the American College of*
1193 *Cardiology* vol. 47 1777–1785 (2006).
1194 9. Bergmann, O., Zdunek, S., Felker, A., Salehpour, M., Alkass, K., Bernard, S.,
1195 Sjostrom, S. L., Szewczykowska, M., Jackowska, T., dos Remedios, C., Malm,
1196 T., Andrä, M., Jashari, R., Nyengaard, J. R., Possnert, G., Jovinge, S., Druid,
1197 H. & Frisén, J. Dynamics of Cell Generation and Turnover in the Human Heart.
1198 *Cell* **161**, 1566–1575 (2015).
1199 10. Pfeffer, M. A. & Braunwald, E. Ventricular remodeling after myocardial
1200 infarction. Experimental observations and clinical implications. *Circulation* **81**,
1201 1161–72 (1990).
1202 11. Richardson, W. J., Clarke, S. A., Quinn, T. A. & Holmes, J. W. Physiological
1203 Implications of Myocardial Scar Structure. *Compr. Physiol.* **5**, 1877–909
1204 (2015).
1205 12. Jopling, C., Sleep, E., Raya, M., Martí, M., Raya, A. & Belmonte, J. C. I.
1206 Zebrafish heart regeneration occurs by cardiomyocyte dedifferentiation and
1207 proliferation. *Nature* **464**, 606–609 (2010).
1208 13. Kikuchi, K., Holdway, J. E., Werdich, A. A., Anderson, R. M., Fang, Y.,
1209 Egnaczyk, G. F., Evans, T., MacRae, C. A., Stainier, D. Y. R. & Poss, K. D.
1210 Primary contribution to zebrafish heart regeneration by gata4+
1211 cardiomyocytes. *Nature* **464**, 601–605 (2010).
1212 14. González-rosa, J. M., Martín, V., Peralta, M., Torres, M. & Mercader, N.
1213 Extensive scar formation and regression during heart regeneration after
1214 cryoinjury in zebrafish. **1674**, 1663–1674 (2011).
1215 15. Aurora, A. B., Porrello, E. R., Tan, W., Mahmoud, A. I., Hill, J. A., Bassel-duby,
1216 R., Sadek, H. A. & Olson, E. N. Macrophages are required for neonatal heart
1217 regeneration. **124**, (2014).
1218 16. Godwin, J. W., Debuque, R., Salimova, E. & Rosenthal, N. A. Heart

1219 regeneration in the salamander relies on macrophage-mediated control of
1220 fibroblast activation and the extracellular landscape. *npj Regen. Med.* **2**, 22
1221 (2017).
1222 17. Lai, S.-L., Marín-Juez, R., Moura, P. L., Kuenne, C., Lai, J. K. H., Tsedeke, A.
1223 T., Guenther, S., Looso, M. & Stainier, D. Y. Reciprocal analyses in zebrafish
1224 and medaka reveal that harnessing the immune response promotes cardiac
1225 regeneration. *Elife* **6**, (2017).
1226 18. Tsarouchas, T. M., Wehner, D., Cavone, L., Munir, T., Keatinge, M.,
1227 Lambertus, M., Underhill, A., Barrett, T., Kassapis, E., Ogryzko, N., Feng, Y.,
1228 van Ham, T. J., Becker, T. & Becker, C. G. Dynamic control of proinflammatory
1229 cytokines Il-1β and Tnf-α by macrophages in zebrafish spinal cord
1230 regeneration. *Nat. Commun.* **9**, 4670 (2018).
1231 19. Nahrendorf, M., Swirski, F. K., Aikawa, E., Stangenberg, L., Wurdinger, T.,
1232 Figueiredo, J.-L., Libby, P., Weissleder, R. & Pittet, M. J. The healing
1233 myocardium sequentially mobilizes two monocyte subsets with divergent and
1234 complementary functions. *J. Exp. Med.* **204**, 3037–3047 (2007).
1235 20. Sager, H. B., Hulsmans, M., Lavine, K. J., Moreira, M. B., Heidt, T., Courties,
1236 G., Sun, Y., Iwamoto, Y., Tricot, B., Khan, O. F., Dahlman, J. E., Borodovsky,
1237 A., Fitzgerald, K., Anderson, D. G., Weissleder, R., Libby, P., Swirski, F. K. &
1238 Nahrendorf, M. Proliferation and Recruitment Contribute to Myocardial
1239 Macrophage Expansion in Chronic Heart Failure. *Circ. Res.* **119**, 853–64
1240 (2016).
1241 21. Nahrendorf, M. & Swirski, F. K. Monocyte and Macrophage Heterogeneity in
1242 the Heart. **02114**, 1624–1634 (2013).
1243 22. Lavin, Y., Winter, D., Blecher-Gonen, R., David, E., Keren-Shaul, H., Merad,
1244 M., Jung, S. & Amit, I. Tissue-Resident Macrophage Enhancer Landscapes
1245 Are Shaped by the Local Microenvironment. *Cell* **159**, 1312–1326 (2014).
1246 23. Sanz-Morejón, A., García-Redondo, A. B., Reuter, H., Marques, I. J., Bates,
1247 T., Galardi-Castilla, M., Große, A., Manig, S., Langa, X., Ernst, A., Piragyte, I.,
1248 Botos, M.-A., González-Rosa, J. M., Ruiz-Ortega, M., Briones, A. M., Salaices,
1249 M., Englert, C. & Mercader, N. Wilms Tumor 1b Expression Defines a Pro-
1250 regenerative Macrophage Subtype and Is Required for Organ Regeneration in
1251 the Zebrafish. *Cell Rep.* **28**, 1296-1306.e6 (2019).
1252 24. Nguyen-Chi, M., , B´eryl Laplace-BuilheTravnickova, J., Luz-crawford, P.,

1253 Tejedor, G., Phan, Q. T., Duroux-richard, I., Levraud, J., Kissa, K., Lutfalla, G.,
1254 Jorgensen, C., Djouad, F., Laplace-Builhe, B., Travnickova, J., Luz-crawford,
1255 P., Tejedor, G., Phan, Q. T., Duroux-richard, I., Levraud, J., Kissa, K., Lutfalla,
1256 G., Jorgensen, C. & Djouad, F. Identification of polarized macrophage subsets
1257 in zebrafish. *Elife* **4**, 1–14 (2015).
1258 25. Matrone, G., Taylor, J., Wilson, K., … J. B.-I. journal of & 2013, undefined.
1259 Laser-targeted ablation of the zebrafish embryonic ventricle: a novel model of
1260 cardiac injury and repair. *Elsevier*.
1261 26. Kaveh, A., Bruton, F. A., Buckley, C., Oremek, M. E. M., Tucker, C. S., Mullins,
1262 J. J., Taylor, J. M., Rossi, A. G. & Denvir, M. A. Live Imaging of Heart Injury in
1263 Larval Zebrafish Reveals a Multi-Stage Model of Neutrophil and Macrophage
1264 Migration. *Front. Cell Dev. Biol.* **8**, 579943 (2020).
1265 27. Shiau, C. E., Kaufman, Z., Meireles, A. M. & Talbot, W. S. Differential
1266 Requirement for irf8 in Formation of Embryonic and Adult Macrophages in
1267 Zebrafish. *PLoS One* **10**, 1–15 (2015).
1268 28. Hume, D. A., Wollscheid-Lengeling, E., Rojo, R. & Pridans, C. The evolution of
1269 the macrophage-specific enhancer (Fms intronic regulatory element) within the
1270 CSF1R locus of vertebrates. *Sci. Rep.* **7**, 1–10 (2017).
1271 29. Bevan, L., Lim, Z. W., Venkatesh, B., Riley, P. R., Martin, P. & Richardson, R.
1272 J. Specific macrophage populations promote both cardiac scar deposition and
1273 subsequent resolution in adult zebrafish. *Cardiovasc. Res.* (2019)
1274 doi:10.1093/cvr/cvz221.
1275 30. Taylor, J. M., Nelson, C. J., Bruton, F. A., Baghbadrani, A. K., Buckley, C.,
1276 Tucker, C. S., Rossi, A. G., Mullins, J. J. & Denvir, M. A. Adaptive prospective
1277 optical gating enables day-long 3D time-lapse imaging of the beating
1278 embryonic zebrafish heart. *Nat. Commun.* **10**, 1–15 (2019).
1279 31. Krijnen, P. A. J., Nijmeijer, R., Meijer, C. J. L. M., Visser, C. A., Hack, C. E. &
1280 Niessen, H. W. M. Apoptosis in myocardial ischaemia and infarction. *J. Clin.*
1281 *Pathol.* **55**, 801–11 (2002).
1282 32. Pisharath, H., Rhee, J. M., Swanson, M. A., Leach, S. D. & Parsons, M. J.
1283 Targeted ablation of beta cells in the embryonic zebrafish pancreas using E.
1284 coli nitroreductase. *Mech. Dev.* **124**, 218–229 (2007).
1285 33. Karra, R., Foglia, M. J., Choi, W.-Y., Belliveau, C., DeBenedittis, P. & Poss, K.
1286 D. Vegfaa instructs cardiac muscle hyperplasia in adult zebrafish. *Proc. Natl.*

1287 *Acad. Sci. U. S. A.* 201722594 (2018) doi:10.1073/pnas.1722594115.
1288 34. Chimote, G., Sreenivasan, J., Pawar, N., Subramanian, J., Sivaramakrishnan,
1289 H. & Sharma, S. Comparison of effects of anti-angiogenic agents in the
1290 zebrafish efficacy-toxicity model for translational anti-angiogenic drug
1291 discovery. *Drug Des. Devel. Ther.* **8**, 1107–1123 (2014).
1292 35. Gemberling, M., Karra, R., Dickson, A. L. & Poss, K. D. Nrg1 is an injury-
1293 induced cardiomyocyte mitogen for the endogenous heart regeneration
1294 program in zebrafish. 1–17 (2015) doi:10.7554/eLife.05871.
1295 36. Honkoop, H., Bakker, D. E. de, Aharonov, A., Kruse, F., Shakked, A., Nguyen,
1296 P. D., Heus, C. de, Garric, L., Muraro, M. J., Shoffner, A., Tessadori, F.,
1297 Peterson, J. C., Noort, W., Bertozzi, A., Weidinger, G., Posthuma, G., Grün,
1298 D., Laarse, W. J. van der, Klumperman, J., Jaspers, R. T., Poss, K. D.,
1299 Oudenaarden, A. van, Tzahor, E., Bakkers, J., de Bakker, D. E., Aharonov, A.,
1300 Kruse, F., Shakked, A., Nguyen, P. D., de Heus, C., Garric, L., Muraro, M. J.,
1301 Shoffner, A., Tessadori, F., Peterson, J. C., Noort, W., Bertozzi, A., Weidinger,
1302 G., Posthuma, G., Grun, D., van der Laarse, W. J., Klumperman, J., Jaspers,
1303 R. T., Poss, K. D., van Oudenaarden, A., Tzahor, E. & Bakkers, J. Single-cell
1304 analysis uncovers that metabolic reprogramming by ErbB2 signaling is
1305 essential for cardiomyocyte proliferation in the regenerating heart. *Elife* **8**,
1306 (2019).
1307 37. Uribe, V., Ramadass, R., Dogra, D., Rasouli, S. J., Gunawan, F., Nakajima, H.,
1308 Chiba, A., Reischauer, S., Mochizuki, N. & Stainier, D. Y. R. In vivo analysis of
1309 cardiomyocyte proliferation during trabeculation. (2018)
1310 doi:10.1242/dev.164194.
1311 38. Zhao, L., Ben-Yair, R., Burns, C. E. & Burns, C. G. Endocardial Notch
1312 Signaling Promotes Cardiomyocyte Proliferation in the Regenerating Zebrafish
1313 Heart through Wnt Pathway Antagonism. *Cell Rep.* **26**, 546-554.e5 (2019).
1314 39. Dovey, H. F., John, V., Anderson, J. P., Chen, L. Z., De Saint Andrieu, P.,
1315 Fang, L. Y., Freedman, S. B., Folmer, B., Goldbach, E., Holsztynska, E. J., Hu,
1316 K. L., Johnson-Wood, K. L., Kennedy, S. L., Kholodenko, D., Knops, J. E.,
1317 Latimer, L. H., Lee, M., Liao, Z., Lieberburg, I. M., Motter, R. N., Mutter, L. C.,
1318 Nietz, J., Quinn, K. P., Sacchi, K. L., Seubert, P. A., Shopp, G. M., Thorsett, E.
1319 D., Tung, J. S., Wu, J., Yang, S., Yin, C. T., Schenk, D. B., May, P. C., Altstiel,
1320 L. D., Bender, M. H., Boggs, L. N., Britton, T. C., Clemens, J. C., Czilli, D. L.,

1321 Dieckman-McGinty, D. K., Droste, J. J., Fuson, K. S., Gitter, B. D., Hyslop, P.
1322 A., Johnstone, E. M., Li, W. Y., Little, S. P., Mabry, T. E., Miller, F. D., Ni, B.,
1323 Nissen, J. S., Porter, W. J., Potts, B. D., Reel, J. K., Stephenson, D., Su, Y.,
1324 Shipley, L. A., Whitesitt, C. A., Yin, T. & Audia, J. E. Functional gamma-
1325 secretase inhibitors reduce beta-amyloid peptide levels in brain. *J.*
1326 *Neurochem.* **76**, 173–181 (2001).
1327 40. Micchelli, C. A., Esler, W. P., Kimberly, W. T., Jack, C., Berezovska, O.,
1328 Kornilova, A., Hyman, B. T., Perrimon, N. & Wolfe, M. S. Gamma-
1329 secretase/presenilin inhibitors for Alzheimer's disease phenocopy Notch
1330 mutations in Drosophila. *FASEB J.* **17**, 79–81 (2003).
1331 41. Geling, A., Steiner, H., Willem, M., Bally-Cuif, L. & Haass, C. A γ-secretase
1332 inhibitor blocks Notch signaling in vivo and causes a severe neurogenic
1333 phenotype in zebrafish. *EMBO Rep.* **3**, 688–694 (2002).
1334 42. Lyons, D. A., Pogoda, H. M., Voas, M. G., Woods, I. G., Diamond, B., Nix, R.,
1335 Arana, N., Jacobs, J. & Talbot, W. S. erbb3 and erbb2 are essential for
1336 Schwann cell migration and myelination in zebrafish. *Curr. Biol.* **15**, 513–524
1337 (2005).
1338 43. Samsa, L. A., Givens, C., Tzima, E., Stainier, D. Y. R., Qian, L. & Liu, J.
1339 Cardiac contraction activates endocardial Notch signaling to modulate
1340 chamber maturation in zebrafish. *Development* **142**, 4080–4091 (2015).
1341 44. Gálvez-Santisteban, M., Chen, D., Zhang, R., Serrano, R., Nguyen, C., Zhao,
1342 L., Nerb, L., Masutani, E. M., Vermot, J., Burns, C. G., Burns, C. E., del Álamo,
1343 J. C. & Chi, N. C. Hemodynamic-mediated endocardial signaling controls in
1344 vivo myocardial reprogramming. *Elife* **8**, (2019).
1345 45. Kuil, L. E., Oosterhof, N., Ferrero, G., Mikulášová, T., Hason, M., Dekker, J.,
1346 Rovira, M., van der Linde, H. C., van Strien, P. M. H., de Pater, E., Schaaf, G.,
1347 Bindels, E. M. J., Wittamer, V. & van Ham, T. J. Zebrafish macrophage
1348 developmental arrest underlies depletion of microglia and reveals Csf1r-
1349 independent metaphocytes. *Elife* **9**, (2020).
1350 46. Lin, X., Zhou, Q., Zhao, C., Lin, G., Xu, J. & Wen, Z. An Ectoderm-Derived
1351 Myeloid-like Cell Population Functions as Antigen Transporters for Langerhans
1352 Cells in Zebrafish Epidermis. *Dev. Cell* **49**, 605-617.e5 (2019).
1353 47. Koth, J., Wang, X., Killen, A. C., Stockdale, W. T., Potts, H. G., Jefferson, A.,
1354 Bonkhofer, F., Riley, P. R., Patient, R. K., Göttgens, B. & Mommersteeg, M. T.

1355 M. Runx1 promotes scar deposition and inhibits myocardial proliferation and
1356 survival during zebrafish heart regeneration. *Development* **147**, (2020).
1357 48. Herrgen, L., Voss, O. P. & Akerman, C. J. Calcium-Dependent Neuroepithelial
1358 Contractions Expel Damaged Cells from the Developing Brain. *Dev. Cell* **31**,
1359 599–613 (2014).
1360 49. Leor, J., Palevski, D., Amit, U. & Konfino, T. Seminars in Cell & Developmental
1361 Biology Macrophages and regeneration : Lessons from the heart. *Semin. Cell*
1362 *Dev. Biol.* **58**, 26–33 (2016).
1363 50. Beisaw, A., Kuenne, C., Günther, S., Dallmann, J., Wu, C.-C., Bentsen, M.,
1364 Looso, M. & Stainier, D. AP-1 Contributes to Chromatin Accessibility to
1365 Promote Sarcomere Disassembly and Cardiomyocyte Protrusion during
1366 Zebrafish Heart Regeneration. *Circ. Res.* CIRCRESAHA.119.316167 (2020)
1367 doi:10.1161/CIRCRESAHA.119.316167.
1368 51. Morikawa, Y., Zhang, M., Heallen, T., Leach, J., Tao, G., Xiao, Y., Bai, Y., Li,
1369 W., Willerson, J. T. & Martin, J. F. Actin cytoskeletal remodeling with protrusion
1370 formation is essential for heart regeneration in Hippo-deficient mice. *Sci.*
1371 *Signal.* **8**, (2015).
1372 52. Marín-juez, R., Marass, M., Gauvrit, S., Rossi, A., Lai, S. & Materna, S. C. Fast
1373 revascularization of the injured area is essential to support zebrafish heart
1374 regeneration. **113**, (2016).
1375 53. Stevens, S. M., von Gise, A., VanDusen, N., Zhou, B. & Pu, W. T. Epicardium
1376 is required for cardiac seeding by yolk sac macrophages, precursors of
1377 resident macrophages of the adult heart. *Dev. Biol.* **413**, 153–159 (2016).
1378 54. Deniset, J. F., Belke, D., Lee, W.-Y., Weber, G. F., Fedak, P. W. M. & Kubes,
1379 P. Gata6+ Pericardial Cavity Macrophages Relocate to the Injured Heart and
1380 Prevent Cardiac Fibrosis. *Immunity* **51**, 131-140.e5 (2019).
1381 55. Zhao, L., Ben-Yair, R., Burns, C. E. G. & Burns, C. E. G. Endocardial Notch
1382 Signaling Promotes Cardiomyocyte Proliferation in the Regenerating Zebrafish
1383 Heart through Wnt Pathway Antagonism. *Cell Rep.* **26**, 546-554.e5 (2019).
1384 56. Zhao, L., Borikova, A. L., Ben-Yair, R., Guner-Ataman, B., MacRae, C. A., Lee,
1385 R. T., Geoffrey Burns, C. & Burns, C. E. Notch signaling regulates
1386 cardiomyocyte proliferation during zebrafish heart regeneration. *Proc. Natl.*
1387 *Acad. Sci. U. S. A.* **111**, 1403–1408 (2014).
1388 57. Raya, A., Koth, C. M., Büscher, D., Kawakami, Y., Itoh, T., Raya, R. M.,

1389 Sternik, G., Tsai, H.-J., Rodríguez-Esteban, C. & Izpisúa-Belmonte, J. C.
1390 Activation of Notch signaling pathway precedes heart regeneration in
1391 zebrafish. *Proc. Natl. Acad. Sci. U. S. A.* **100 Suppl 1**, 11889–95 (2003).
1392 58. Zhao, L., Ben-Yair, R., Burns, C. G. E. G. & Burns, C. G. E. G. Endocardial
1393 Notch Signaling Promotes Cardiomyocyte Proliferation in the Regenerating
1394 Zebrafish Heart through Wnt Pathway Antagonism. *Cell Rep.* **26**, 546-554.e5
1395 (2019).
1396 59. Gemberling, M., Karra, R., Dickson, A. L. & Poss, K. D. Nrg1 is an injury-
1397 induced cardiomyocyte mitogen for the endogenous heart regeneration
1398 program in zebrafish. *Elife* **4**, (2015).
1399 60. Huang, C. J., Tu, C. T., Hsiao, C. Der, Hsieh, F. J. & Tsai, H. J. Germ-line
1400 transmission of a myocardium-specific GFP transgene reveals critical
1401 regulatory elements in the cardiac myosin light chain 2 promoter of zebrafish.
1402 *Dev. Dyn.* **228**, 30–40 (2003).
1403 61. Yoo, S. K., Deng, Q., Cavnar, P. J., Wu, Y. I., Hahn, K. M. & Huttenlocher, A.
1404 Differential Regulation of Protrusion and Polarity by PI(3)K during Neutrophil
1405 Motility in Live Zebrafish. *Dev. Cell* **18**, 226–236 (2010).
1406 62. Ellett, F., Pase, L., Hayman, J. W., Andrianopoulos, A. & Lieschke, G. J.
1407 mpeg1 promoter transgenes direct macrophage-lineage expression in
1408 zebrafish. *Blood* **117**, e49 (2011).
1409 63. Renshaw, S. A., Loynes, C. A., Trushell, D. M. I., Elworthy, S., Ingham, P. W.
1410 & Whyte, M. K. B. A transgenic zebrafish model of neutrophilic inflammation.
1411 *Blood* **108**, 3976–3978 (2006).
1412 64. Mickoleit, M., Schmid, B., Weber, M., Fahrbach, F. O., Hombach, S.,
1413 Reischauer, S. & Huisken, J. High-resolution reconstruction of the beating
1414 zebrafish heart. *Nat. Methods* **11**, 919–922 (2014).
1415 65. Lin, Y.-F., Swinburne, I. & Yelon, D. Multiple influences of blood flow on
1416 cardiomyocyte hypertrophy in the embryonic zebrafish heart. *Dev. Biol.* **362**,
1417 242–253 (2012).
1418 66. Gray, C., Loynes, C. A., Whyte, M. K. B., Crossman, D. C., Renshaw, S. A. &
1419 Chico, T. J. A. Simultaneous intravital imaging of macrophage and neutrophil
1420 behaviour during inflammation using a novel transgenic zebrafish. 811–819
1421 (2011) doi:10.1160/TH10-08-0525.
1422 67. Davison, J. M., Akitake, C. M., Goll, M. G., Rhee, J. M., Gosse, N., Baier, H.,

1423 Halpern, M. E., Leach, S. D. & Parsons, M. J. Transactivation from Gal4-VP16
1424 transgenic insertions for tissue-specific cell labeling and ablation in zebrafish.
1425 *Dev. Biol.* **304**, 811–824 (2007).
1426 68. Rottbauer, W., Saurin, A. J., Lickert, H., Shen, X., Burns, C. G., Wo, Z. G.,
1427 Kemler, R., Kingston, R., Wu, C. & Fishman, M. Reptin and pontin
1428 antagonistically regulate heart growth in zebrafish embryos. *Cell* **111**, 661–672
1429 (2002).
1430 69. Ninov, N., Borius, M. & Stainier, D. Y. R. Different levels of Notch signaling
1431 regulate quiescence, renewal and differentiation in pancreatic endocrine
1432 progenitors. *Development* **139**, 1557–1567 (2012).
1433 70. Chi, N. C., Shaw, R. M., De Val, S., Kang, G., Jan, L. Y., Black, B. L. &
1434 Stainier, D. Y. R. Foxn4 directly regulates tbx2b expression and
1435 atrioventricular canal formation. *Genes Dev.* **22**, 734–739 (2008).
1436 71. Choi, J., Dong, L., Ahn, J., Dao, D., Hammerschmidt, M. & Chen, J. N. FoxH1
1437 negatively modulates flk1 gene expression and vascular formation in zebrafish.
1438 *Dev. Biol.* **304**, 735–744 (2007).
1439 72. Kikuchi, K., Gupta, V., Wang, J., Holdway, J. E., Wills, A. A., Fang, Y. & Poss,
1440 K. D. tcf21+ epicardial cells adopt non-myocardial fates during zebrafish heart
1441 development and regeneration. *Development* **138**, 2895–902 (2011).
1442 73. Mickoleit, M., Schmid, B., Weber, M., Fahrbach, F. O., Hombach, S.,
1443 Reischauer, S. & Huisken, J. High-resolution reconstruction of the beating
1444 zebrafish heart. *Nat. Methods* **11**, 919–922 (2014).
1445 74. Schindelin, J., Arganda-Carreras, I., Frise, E., Kaynig, V., Longair, M.,
1446 Pietzsch, T., Preibisch, S., Rueden, C., Saalfeld, S., Schmid, B., Tinevez, J.
1447 Y., White, D. J., Hartenstein, V., Eliceiri, K., Tomancak, P. & Cardona, A. Fiji:
1448 An open-source platform for biological-image analysis. *Nature Methods* vol. 9
1449 676–682 (2012).
1450 75. Burns, C. G. & MacRae, C. A. Purification of hearts from zebrafish embryos.
1451 *BioTechniques* vol. 40 274–282 (2006).
1452
1453
1454 **Videos:**
1455
1456 Videos 1-8 can be found deposited on Dropbox via the following link:

https://www.dropbox.com/sh/xy5re3qvf4oc327/AAAVYj6SlCxZBJGKKYQLNI6Ia?dl=0

Video 1: LSFM-acquired heartbeat-synchronised time-lapse of a *Tg(csf1ra:mCherry;mpeg1:GFP)* heart showing macrophage heterogeneity following cardiac injury.

Video 2: LSFM-acquired heartbeat-synchronised time-lapse of a *Tg(mpeg1:mCherry;tnfa:GFP)* heart showing macrophage plasticity following cardiac injury.

Video 3: LSFM-acquired heartbeat-synchronised time-lapse of a *Tg(myl7:h2b-GFP;myl7:mKateCAAX)* heart following cardiac injury showing cardiomyocyte apoptosis following injury.

Video 4: LSFM-acquired heartbeat-synchronised time-lapse of a *Tg(myl7:h2b-GFP;mpeg1:GFP)* heart injected with propdium iodide showing PI+ cardiomyocyte expulsion following cardiac injury.

Video 5: LSFM-acquired heartbeat-synchronised time-lapse of a *Tg(myl7:GFP;mpeg1:mCherry)* heart, 3D surface rendered, showing removal and internalization of myocardial debris by macrophages following injury.

Video 6: LSFM-acquired heartbeat-synchronised time-lapse of a *Tg(myl7:GFP)* heart, 3D surface rendered, showing budding and bridging of wound margin myocardium following injury.

Video 7: LSFM-acquired heartbeat-synchronised time-lapse of a *Tg(myl7:h2b-GFP;myl7:mKateCAAX)* heart, showing budding and bridging of individual wound-margin cardiomyocytes following injury.

Video 8: LSFM-acquired heartbeat-synchronised time-lapse of a *Tg(myl7:h2b-GFP;myl7:mKateCAAX)* heart, showing cardiomyocyte cell division with nuclear division and cytokinesis.